JOURNAL OF SURGICAL RESEARCH 179 (2013) 24–32

Available online at www.sciencedirect.com

SciVerse ScienceDirect

journal homepage: www.JournalofSurgicalResearch.com

Membranous expression of activated leukocyte cell adhesion molecule contributes to poor prognosis and malignant phenotypes of non–small-cell lung cancer

Futoshi Ishiguro, MD,[a,b] Hideki Murakami, MD,[a] Tetsuya Mizuno, MD,[a,b] Makiko Fujii, DDS,[a] Yutaka Kondo, MD,[a] Noriyasu Usami, MD,[b] Tetsuo Taniguchi, MD,[b] Kohei Yokoi, MD,[b] Hirotaka Osada, MD,[a,c] and Yoshitaka Sekido, MD[a,c,]*

[a] *Division of Molecular Oncology, Aichi Cancer Center Research Institute, Nagoya, Japan*

[b] *Department of Thoracic Surgery, Nagoya University Graduate School of Medicine, Nagoya, Japan*

[c] *Program in Function Construction Medicine, Department of Cancer Genetics, Nagoya University Graduate School of Medicine, Nagoya, Japan*

ARTICLE INFO

Article history:
Received 20 May 2012
Received in revised form
8 August 2012
Accepted 22 August 2012
Available online 7 September 2012

Keywords:
Activated leukocyte cell adhesion molecule
Immunohistochemistry
Non–small-cell lung cancer
Prognosis

ABSTRACT

Background: Activated leukocyte cell adhesion molecule (ALCAM) has been shown to correlate with the prognosis of patients with various types of human malignancies. However, the relationship between ALCAM expression and progression of non–small-cell lung cancer (NSCLC) has not been investigated. This study was designed to clarify the prognostic impact of ALCAM expression of NSCLC cells.

Materials and methods: The study population consisted of 147 NSCLC patients who underwent complete resection. We performed immunohistochemical staining for ALCAM expression and correlated this to the clinicopathologic parameters and patient survival. The ALCAM expression in NSCLC cell lines was analyzed using quantitative reverse transcription–polymerase chain reaction and Western blot analyses. ALCAM knockdown in NSCLC cell lines was performed with lentivirus-mediated short hairpin RNA transduction.

Results: Positive membranous and cytoplasmic ALCAM expressions were detected in 66 (44.9%) and 57 (38.8%) patients, respectively. A significant association of high membranous ALCAM expression with shortened overall survival (OS) was found ($P = 0.009$). However, patients with cytoplasmic staining of ALCAM showed no significantly shortened OS ($P = 0.723$). Multivariate analyses showed that membranous expression was adverse prognostic factors for OS (hazard ratio, 2.11; $P = 0.046$). ALCAM knockdown with short hairpin RNA suppressed cell migration and invasion of NSCLC cell lines *in vitro*.

Conclusions: Strong membranous ALCAM expression is associated with a poor prognosis in patients with resected NSCLC, and overexpression of ALCAM causes malignant phenotypes of NSCLC.

1. Introduction

Lung cancer is the most common cause of death from cancer [1]. Non–small-cell lung cancer (NSCLC) accounts for approximately 85% of all lung cancers. Despite the progress of treatment modalities in the past decade, the 5-y survival rate of NSCLC patients with surgical treatment remains only 69.6% [2]. Better understanding of the molecular features of NSCLC

* *Corresponding author.* Division of Molecular Oncology, Aichi Cancer Center Research Institute, 1-1 Kanokoden, Chikusa-ku, Nagoya, Aichi 464-8681, Japan. Tel.: +81 52 764 2983; fax: +81 52 764 2993.
E-mail address: ysekido@aichi-cc.jp (Y. Sekido).

0022-4804/$ – see front matter © 2013 Elsevier Inc. All rights reserved.
http://dx.doi.org/10.1016/j.jss.2012.08.044

would help to identify an effective therapeutic target of this malignant tumor. Regarding the prognostic indicators of NSCLC, the pathologic stage has been consistently shown to be the best predictor for prognosis [3]. Although other clinical factors including gender, age, and smoking history have also been shown to be a possible prognostic factor for NSCLC patients, further development of novel biological or genetic factors would become an aid for predicting NSCLC patient prognosis more precisely.

Activated leukocyte cell adhesion molecule (ALCAM or CD166) belongs to the immunoglobulin superfamily, which mediates both heterophilic (ALCAM–CD6) and homophilic (ALCAM–ALCAM) cell–cell interactions [4]. ALCAM has been reported to promote cell migration [5,6] and angiogenesis [7] *in vitro* and be involved in invasion and metastases of primary tumors [8,9]. Since its discovery, ALCAM has also been shown as a prognostic marker in colorectal cancer [10], gastric cancer [11], and various types of malignant tumors [12–17]. However, the relationship between the ALCAM expression and malignant phenotypes of NSCLC has not been reported.

The aim of this study was to evaluate the prognostic significance of ALCAM in NSCLC, which has not been explored to date. We investigated the expression of ALCAM in a cohort of clinically characterized NSCLC by immunohistochemistry (IHC) and correlated that with clinicopathologic features. Moreover, we knocked down ALCAM in NSCLC cell lines to evaluate its effects on malignant phenotypes of NSCLC *in vitro*.

Table 1 – Clinicopathologic characteristics of 147 patients with NSCLC.

Variables	Number of patients (*n*)	%
Total, *N*	147	
Age (y)		
Median (range)	68 (35–84)	
Sex		
Female	48	32.7
Male	99	67.3
Smoking status		
Pack-years ≥20	58	39.5
<20	89	60.5
CEA (ng/mL)*		
≥5	88	62.4
<5	53	37.6
Histology		
Adenocarcinoma	101	68.7
Squamous cell carcinoma	40	27.2
Other	6	4.1
Pathologic stage		
I	93	63.3
II	33	22.4
III	21	14.3
Operation		
Lobectomy	122	83.0
Bilobectomy/extended lobectomy	8	5.4
Lobectomy with adjacent organ resection	9	6.2
Pneumonectomy	8	5.4

* Serum CEA levels were not measured in six patients.

2. Materials and methods

2.1. Patient samples

From January 2004 through June 2006, 147 patients had complete resection by lobectomy or pneumonectomy with mediastinal lymph node dissection for primary NSCLC at the Nagoya University Hospital. The clinicopathologic features of patients were summarized in Table 1. Overall survival (OS) was measured from the date of surgery until death or the final date of the follow-up (March 31, 2011). The median length of follow-up for all the patients was 55 mo (range, 4–78 mo), and the median length of follow-up for surviving patients was 61 mo (range, 33–78 mo). Tumors were pathologically staged based on the 7th Edition of the TNM Classification for Lung and Pleural Tumors [18]. The histologic subtype was classified according to the World Health Organization guidelines [19]. The study was approved by the institutional review boards. Written informed consent was obtained before the resection from all the patients regarding tissue sampling.

2.2. IHC analysis

IHC analysis was carried out on formalin-fixed paraffin-embedded tissue sections of tumor samples. Sections (4-μm thick) were deparaffinized in xylene and rehydrated in increasing concentrations of ethanol. The antigens were retrieved by 45-min heating at 98°C in 0.5% Immunosaver (Nisshin EM, Tokyo, Japan) in a water bath. After blocking the endogenous peroxidase activity with 3% aqueous H_2O_2 solution for 15 min, the slides were incubated in blocking solution for 15 min, followed by 1-h incubation at room temperature (RT) with a primary mouse monoclonal anti-ALCAM antibody (clone MOG/07; NovoCastra, Newcastle, UK) at a 1:200 dilution. After washing, the slides were incubated with a biotinylated secondary antibody for 15 min at RT and allowed to react for 15 min with the streptoavidin–peroxidase reagent using an Ultra-tech Kit (Beckman Coulter, Marseille, France). The 3,3′-diaminobenzidine tetrahydrochloride Liquid System (DakoCytomation, Glostrup, Denmark) was used to detect immunostaining. Normal mouse immunoglobulin or omission of the primary antibody served as negative controls (Fig. 1F).

2.3. Positive criterion for IHC staining

ALCAM showed membranous and cytoplasmic staining patterns. The intensity of each membranous and cytoplasmic staining was scored for positivity as follows: 0, no staining or faint staining in <10% of tumor cells; 1+, faint staining in >10% of tumor cells; 2+, weak or moderate staining in >10% of tumor cells; and 3+, >10% of strong staining. Zero or 1+ staining intensity was considered ALCAM negative, and 2+ or 3+ staining intensity was considered positive as reported previously [10,11,16]. Two independent researchers (F.I. and H.M.) blinded to patient characteristics, and outcome evaluated the slides. All cases with discrepant evaluations were discussed during observation with the same microscope, and a consensus was reached.

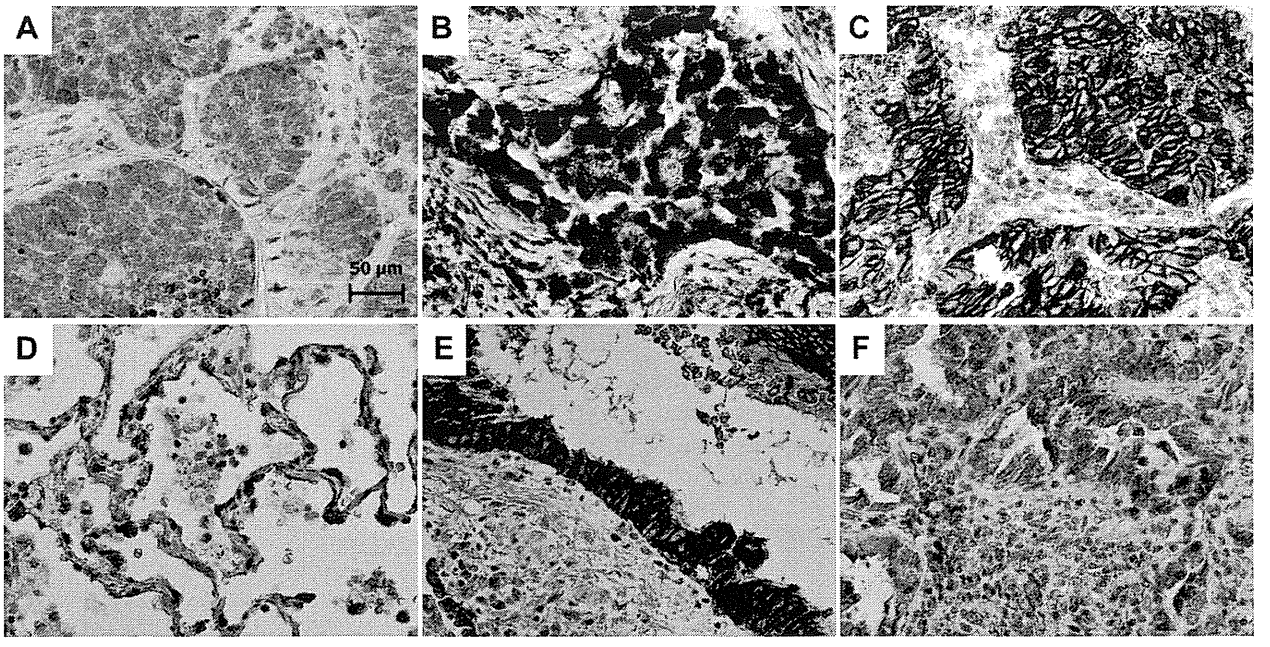

Fig. 1 – IHC analysis of ALCAM in NSCLC and normal lung tissues. (A) NSCLC displaying an ALCAM intensity of 0. (B) NSCLC displaying a cytoplasmic intensity of 3+. (C) NSCLC displaying membranous intensity of 3+. (D) Alveolar epithelial cells with a cytoplasmic ALCAM intensity of 1+. (E) Bronchoepithelial cells with strong membranous immunoreactivity of 3+, which served as a positive control of immunostainings. (F) The same specimen (C) was stained with the omission of primary antibody, which served as negative control. Original magnification, ×400.

2.4. *Cell lines*

The human NSCLC cell lines HCC78 and HCC193 were the kind gift of Dr Adi F. Gazdar. A549, H2228, H596, and NCI-H23 cell lines were purchased from the American Type Culture Collection (ATCC, Rockville, MD). VMRC-LCD was obtained from the Japanese Collection of Research Bioresources (Osaka, Japan). A human bronchial epithelial cell line (BEAS-2B) transformed with SV40 virus was purchased from the ATCC. All the NSCLC cell lines were cultured in RPMI-1640 medium supplemented with 10% fetal calf serum and 1× antibiotic–antimycotic (Invitrogen, Carlsbad, CA) at 37°C in a humidified incubator with 5% CO_2. BEAS-2B was cultured according to the ATCC instructions.

2.5. *Preparation of RNA*

Total RNA was prepared using RNeasy Plus RNA extraction kit (Qiagen, Tokyo, Japan) according to the manufacturer's protocol. Random-primed first-strand complementary DNA was synthesized from 1.0 μg of total RNA using Superscript II according to the manufacturer's instructions (Invitrogen).

2.6. *Quantitative reverse transcription–polymerase chain reaction*

Quantitative reverse transcription–polymerase chain reaction was performed using first-strand complementary DNA with Power SYBR Green PCR Master (Applied Biosystems, Foster City, CA). The amplification was carried out with an ABI 7500 Real-Time PCR system (Applied Biosystems) according to the manufacturer's instructions. *Glyceraldehyde-3-phosphate dehydrogenase* served as an internal control; the expression levels of *ALCAM* in each of the samples were normalized on the basis of the corresponding *glyceraldehyde-3-phosphate dehydrogenase* content and recorded as relative expression levels.

2.7. *Antibodies*

Mouse anti-ALCAM antibody (clone MOG/07 and SNCL-CD166) for Western blot and IHC analyses was purchased from Novocastra. Mouse anti-ALCAM (clone 3A6 and 559260) for immunofluorescence was purchased from BD Bioscience Discovery Labware (Bedford, MA) and mouse anti-β-actin (clone AC74) was from Sigma (St Louis, MO). Rabbit anti-β-catenin antibody (sc-7199) was purchased from Santa Cruz Biotechnology (Santa Cruz, CA).

2.8. *Western blot analysis*

The preparation of total cell lysates and Western blotting were carried out as described previously [20]. In brief, cells growing confluently were rinsed twice with phosphate-buffered saline, lysed in sodium dodecyl sulfate (SDS) sample buffer (62.5 mM Tris, pH 6.8, 2% SDS, 2% 2-mercaptoethanol, and 10% glycerol), and homogenized. Total cell lysate (30 μg) was subjected to SDS–polyacrylamide gel electrophoresis and transferred to Immobilon-P polyvinylidene difluoride membranes (Millipore, Bedford, MA). After blocking with 3% nonfat dry milk, the filters were incubated with the primary antibody, washed with

phosphate-buffered saline, reacted with the secondary antibody, and then detected with enhanced chemiluminescence (Amersham Bioscience, Buckinghamshire, UK).

2.9. *Immunofluorescent microscopic analysis*

Cells were fixed, permeabilized, and incubated with a primary antibody (anti-ALCAM antibody, 2.5 μg/mL and anti-β-catenin antibody, 0.4 μg/mL) for 1 h at RT, followed by incubation with Alexa Fluor 488- or Alexa Fluor 564-conjugated secondary antibodies at RT. Nuclear staining was carried out with 4′, 6-diamidino-2-phenylindole after incubation with secondary antibody. Microscopic observation was carried out using a confocal laser scanning system (LSM510; Carl Zeiss Micro-Imaging GmbH, Jena, Germany) at ×63 magnification, as described previously [21].

2.10. *Construction of RNA interference vectors*

Complementary short hairpin sequence was cloned into pLentiLox3.7 [20] under the control of a U6 promoter and transfected into HEK293FT cells along with the vectors of VSVG, RSV-Rev, and pMDLg-pRPE to generate lentiviruses that transcribe short hairpin RNA. A short hairpin oligonucleotide was designed for sequence within the ALCAM open reading frame (ALCAM-Sh, 5′-GAGGAATCTCCTTATATTA-3′). A control vector, ALCAM-Scr (5′-GTTTACCACGGAATATTAT-3′), was constructed using oligonucleotide with scrambled sequence for ALCAM-Sh. The efficacy of each virus was tested by immunoblotting of whole-cell lysates 96 h after infecting cells at the multiplicity of infection of 10.

2.11. *Cell migration and invasion assays*

Cell migration and invasion potential were measured by *in vitro* Boyden chamber assays (BD Bioscience Discovery Labware) according to the manufacturer's protocol. Briefly, NSCLC cells (5×10^4 for transwell migration assay and 1×10^5 for Matrigel invasion assay) in 0.5 mL of serum-free RPMI-1640 medium were added to the upper wells of Matrigel-uncoated or Matrigel-coated Boyden chambers with 8-μm pore membrane. The bottom chambers were filled with 5% fetal calf serum–containing medium as a chemoattractant. After 22-h incubation, noninvasive cells were removed by scrubbing with a cotton swab. Cells that migrated through the membrane and stuck to the lower surface of the membrane were fixed stained using Diff-Quick stain (Sysmex, Kobe, Japan). Values for migration and invasion were obtained by counting five predetermined fields per membrane at ×100 magnifications, representing the average of three independent experiments.

2.12. *Statistical analysis*

For statistical analysis, chi-square or Fisher exact test was used to assess the significance of associations between the expression of ALCAM and clinicopathologic parameters. Continuous variables were compared using unpaired *t*-test. The Kaplan–Meier method was used to estimate OS curves, and the survival differences were analyzed by the log-rank test. A multivariate analysis was performed using the Cox proportional hazard model to study the effects of variables on survival. The *P* values of all statistical tests were two sided, and the differences were considered significant at *P* values <0.05. All analyses were performed using StatView software (version 5; SAS Institute Inc, Cary, NC).

3. Results

3.1. *IHC analysis of ALCAM in NSCLCs and normal lung tissues*

ALCAM displayed a differential subcellular expression patterns, that is, membranous and cytoplasmic staining (Fig. 1A–C). Positive membranous staining was seen in 66 (44.9%) patients and positive cytoplasmic staining in 57 (38.8%) patients (Table 2). These ALCAM staining patterns were in concordance with IHC patterns in the Human Protein Atlas database (www.proteinatlas.org). Apart from NSCLC cells, alveolar epithelial cells (Fig. 1D), normal mesothelium, and reactive mesothelial cells showed ALCAM intensity of 1+. Bronchoepithelial cells (Fig. 1E), macrophages, and neural cells showed a staining intensity of 3+ in a membranous fashion. We repeated IHC with two different antibodies of ALCAM, primary mouse monoclonal anti-ALCAM antibody (clone MOG/07; NovoCastra) and primary rabbit polyclonal anti-ALCAM antibody (Atlas Antibody AB, Stockholm, Sweden). The expression patterns were identical between the two different antibodies. We then used only the monoclonal antibody for IHC evaluation because it has also been successfully approved in previous reports [10–13,15].

3.2. *ALCAM expression by IHC in correlation with clinicopathologic parameters and prognosis*

We investigated the relationship between the clinicopathologic characteristic of NSCLC and ALCAM IHC staining. No correlations between membranous or cytoplasmic immunoreactivity and clinicopathologic variables were found (Table 3). Figure 2 showed OS stratified by subcellular

Table 2 – Membranous and cytoplasmic staining status of ALCAM.

Cytoplasmic staining	Score	Membranous staining				Total
		Negative		Positive		
		0	1+	2+	3+	
Negative	0	21	7	5	0	33
	1+	11	8	30	8	57
Positive	2+	18	13	18	2	51*
	3+	1	2	3	0	6*
Total		51	30	56†	10†	147

Membranous and cytoplasmic positivities were evaluated separately.
* A total of 57 (38.8%) patients showed cytoplasmic expression.
† A total of 66 (44.9%) patients showed membranous expression.

Table 3 – Patient characteristics stratified ALCAM IHC staining status.

Variables	Number of patients	A			B		
		ALCAM IHC		P value	ALCAM IHC		P value
		Membranous positive	Membranous negative		Cytoplasmic positive	Cytoplasmic negative	
Total	147	66	81		57	90	
Age (y)							
Median (range)		70 (35–84)	67 (40–81)	0.113*	67 (40–80)	69 (35–84)	0.095*
Sex							
Female	48	24	24	0.387†	20	28	0.616†
Male	99	42	57		37	62	
Smoking status							
Pack-years ≥20	58	29	29	0.315†	23	35	0.860†
<20	89	37	52		34	55	
CEA (ng/mL)‡							
≥5	88	33	55	0.118†	35	53	0.642†
<5	53	27	26		19	34	
Histology							
Adenocarcinoma	101	48	53	0.315†	46	55	0.200†
Squamous cell carcinoma	40	17	23		10	30	
Other	6	1	5		1	5	
Pathologic stage							
I	93	42	51	0.979†	38	55	0.093†
II	33	15	18		8	25	
III	21	9	12		11	10	

* Fisher exact or chi-square test.
† Mann–Whitney U-test.
‡ Serum CEA levels were not measured in six patients.

expression patterns of ALCAM. Patients with membranous ALCAM expression showed a significantly shortened OS compared with those tumors showed negative expression ($P = 0.009$). The 5-y survival probabilities were 64.5% for the membranous-positive group and 82.0% for the membranous-negative group (Fig. 2A). In contrast, patients whose tumors showed positive cytoplasmic staining of ALCAM did not have a significant survival difference compared with ALCAM cytoplasmic-negative group ($P = 0.723$) (Fig. 2B).

3.3. *Prognostic values of ALCAM expression*

We analyzed the impact of all variables on OS. Univariate analysis showed a significant prognostic difference with

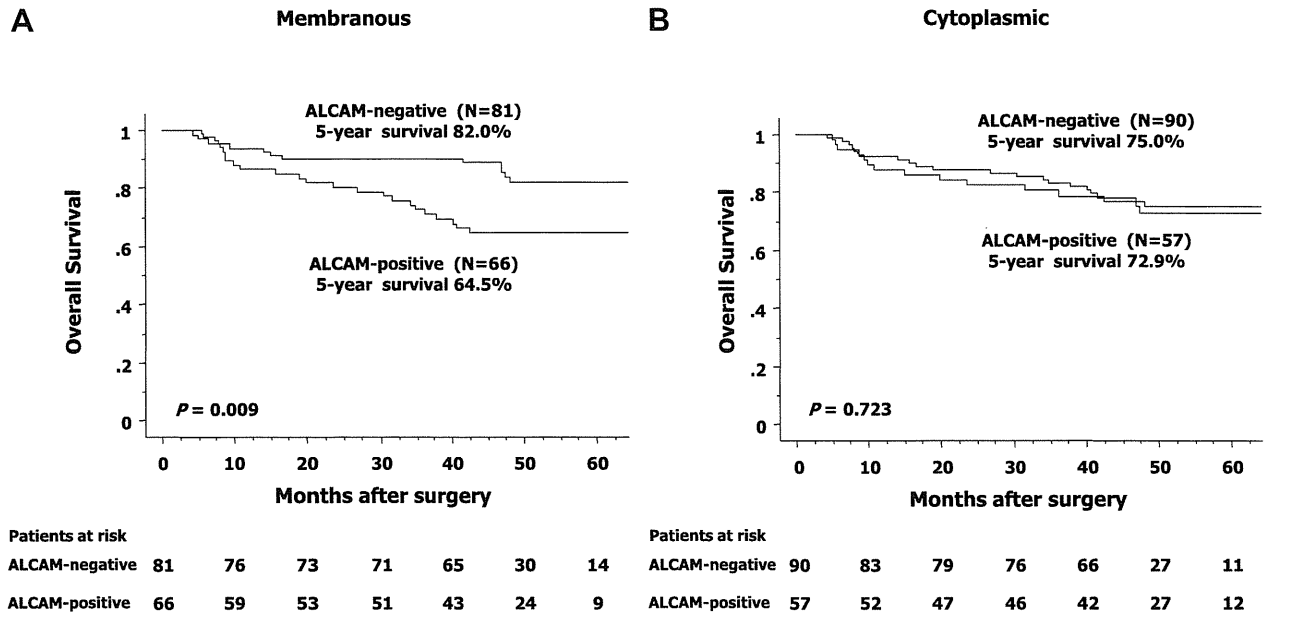

Fig. 2 – Kaplan–Meier survival analysis stratified by positive or negative ALCAM IHC staining according to (A) membranous and (B) cytoplasmic staining.

age, sex, smoking status, serum Carcinoembryonic antigen, histology, pathologic stage, and ALCAM membranous expression (Table 4). As shown in Table 5, multivariate analysis confirmed membranous ALCAM expression as an independent negative prognostic factor (hazard ratio, 2.11; 95% confidence interval, 1.01–4.42, $P = 0.046$). Among the remaining variables, age, sex, serum CEA, and pathologic stage were significant in our patient cohort (Table 5).

3.4. *ALCAM expression in NSCLC cell lines*

We next examined the expression status of ALCAM with quantitative reverse transcription–polymerase chain reaction and Western blot analyses in seven NSCLC cell lines and an immortalized bronchial epithelial cell line, BEAS-2B. Consistent with the result of positive ALCAM staining of bronchoepithelial cells with IHC (Fig. 1E), we found that BEAS-2B also expressed ALCAM. Among the seven NSCLC cell lines, we considered six cell lines expressed relatively high ALCAM messenger RNA (Fig. 3A). Figure 3B showed that ALCAM protein levels determined by Western blot analysis showed a good correlation with messenger RNA in most cell lines. We also performed the immunocytochemical analysis using HCC193 and H596 cells and observed strong signals at cell–cell interaction regions (Fig. 3C).

3.5. *Inhibition of ALCAM suppressed migration and invasion of mesothelioma cells*

To determine whether ALCAM plays a possible role in NSCLC progression, we investigated whether inhibition of ALCAM suppresses malignant phenotypes of NSCLC cells. We selected HCC193 and H596 as representative cell lines with high ALCAM protein expression. We synthesized ALCAM short hairpin RNA constructs and transduced into these cell lines. Efficient depletion of ALCAM expression was confirmed by Western blot analysis (Fig. 4A). ALCAM-depleted cells showed weaker migration and invasion ability compared with control cells (Fig. 4B and C). However, we did not detect the inhibitory effect on cell proliferation by ALCAM knockdown (data not shown).

Table 4 – Univariate analysis of factors associated with patient survival.

Variables	HR	95% CI	P value
Age (continuous)	1.06	1.02–1.11	0.009
Sex			
Female/male	6.37	1.96–20.83	0.002
Smoking status			
Pack-years ≥20/<20	3.10	1.36–7.09	0.007
CEA (ng/mL)*			
≥5/<5	3.53	1.74–7.19	0.001
Histology			
Adenocarcinoma/other	2.18	1.13–4.18	0.020
Pathologic stage			
I/II + III	3.82	1.93–7.52	0.001
ALCAM membranous staining			
Negative/positive	3.56	1.76–7.19	0.012
ALCAM cytoplasmic staining			
Negative/positive	1.13	0.58–2.19	0.723

CI = confidence interval; HR = hazard ratio.
* Serum CEA levels were not measured in six patients.

Table 5 – Multivariate analysis of factors associated with patient survival.

Variables	HR	95% CI	P value
Age (continuous)	1.05	1.00–1.10	0.039
Sex			
Female/male	7.41	1.56–29.52	0.012
Smoking status			
Pack-years ≥20/<20	1.44	0.46–4.48	0.530
CEA (ng/mL)*			
≥5/<5	2.33	1.12–4.87	0.024
Histology			
Adenocarcinoma/others	1.09	0.50–2.37	0.828
Pathologic stage			
I/II + III	3.69	1.75–7.75	0.001
ALCAM membranous staining			
Negative/positive	2.11	1.01–4.42	0.046

CI = confidence interval; HR = hazard ratio.
* Serum CEA levels were not measured in six patients.

4. Discussion

To our knowledge, this is the first report of a retrospective study designed to clarify the possible impact of ALCAM expression on patient outcome in completely surgically resected NSCLC. Among 147 NSCLC patients, 66 (44.9%) tumors showed positive membranous ALCAM staining and 57 (38.8%) showed cytoplasmic ALCAM staining with IHC analysis. We found that the increased membranous, but not cytoplasmic, overexpression of ALCAM was associated with poor prognosis of NSCLC patients.

The association of ALCAM with disease progression in human malignancies has been first suggested in malignant melanoma [9]. Subsequently, as a poor prognostic factor, ALCAM has also been indicated in various types of human malignancies [10–17]. As for its expression in NSCLC, ALCAM was detected as one of the elevated cancer-specific molecules in malignant pleural effusion of NSCLC patients with shotgun mass spectrometry [22]. The levels of ALCAM expression in pleural effusion were correlated with the signal intensities of the primary tumors that were detected with IHC, and the membranous expression of ALCAM was also confirmed in the tumor cells. Recently, ALCAM has been shown to be a cell surface marker, which enriches for cancer stem cells in NSCLC [23] and also to be one of the new potential biomarkers for diagnosis and prognosis of lung cancer [24]. We hypothesized that ALCAM might have a possible impact on NSCLC progression and determined to investigate the correlation between ALCAM expression and NSCLC patient survival.

In this study, we identified two types of ALCAM expression patterns, membranous and cytoplasmic, in NSCLC tumors as reported in other types of malignancies [9–17]. We found that the membranous expression of ALCAM was of prognostic value, whereas the cytoplasmic expression was not. Thus, our

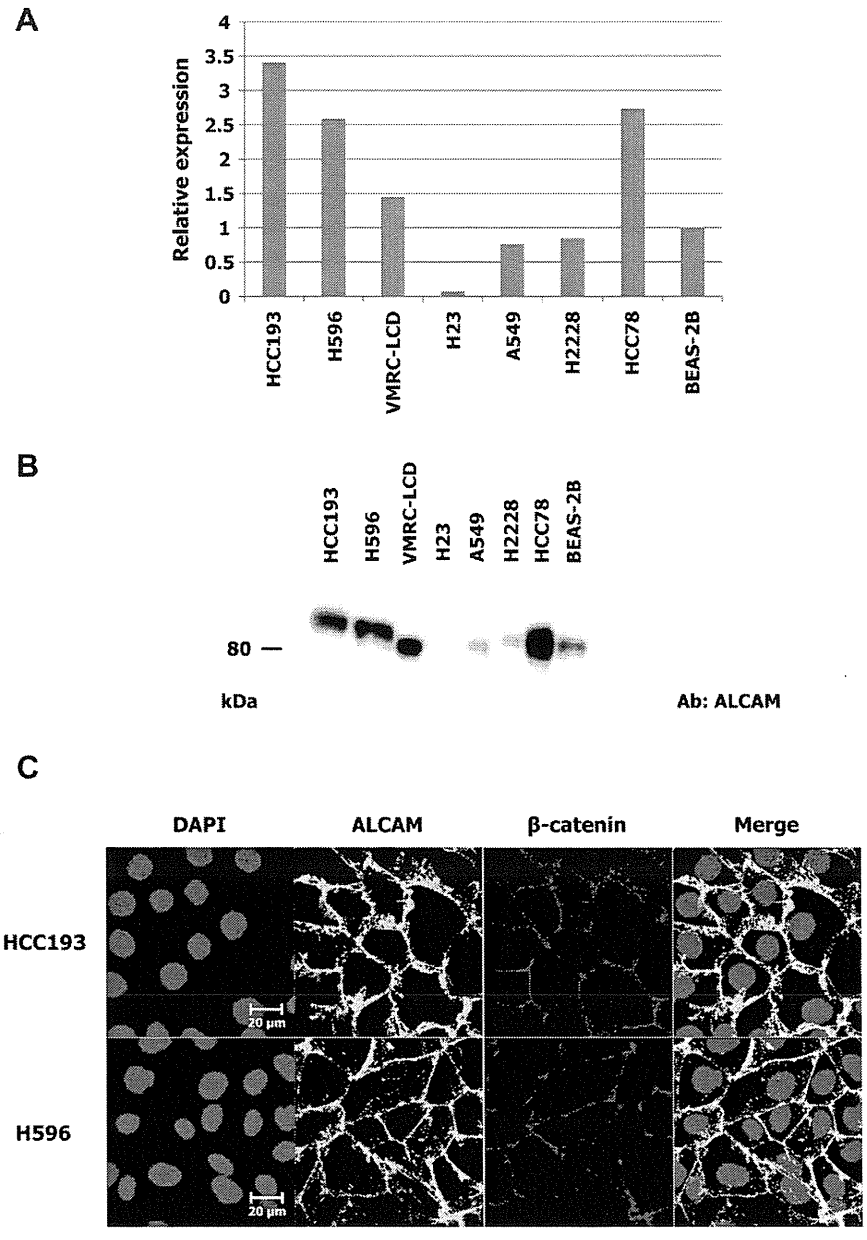

Fig. 3 – The expression of ALCAM in NSCLC cell lines. (A) Quantitative reverse transcription–polymerase chain reaction analysis of ALCAM in seven NSCLC cell lines and one immortalized bronchial epithelial cells, BEAS-2B. The relative expression of BEAS-2B was arbitrarily set as 1.0. (B) Western blot analysis of ALCAM in seven NSCLC cell lines. The expression of β-actin was used as the control. (C) Immunocytochemical analysis. Strong membranous signals of ALCAM were observed in HCC193 and H596 cells. β-Catenin staining was used as the marker of the cell–cell interaction region.

findings suggested that membranous expression of ALCAM in NSCLC cells was also associated with a worse prognosis of patients with NSCLC, similarly to other types of tumors, including melanoma [9], colorectal cancer [10], and gastric cancer [11]. In contrast, the association with an unfavorable prognosis of cytoplasmic ALCAM staining was also suggested in breast cancer [13] and ovarian cancer [15], although we did not confirm this in the present study. Thus, the previous and our studies may indicate that the evaluation of the prognostic impact of ALCAM expression in tumor cells should be considered for each type of tumor based on subcellular localization and expression levels of ALCAM.

With respect to subcellular localization of ALCAM, Tomita *et al.* investigated the relationship between ALCAM and cytoskeleton. They found that loss of α-catenin, which is involved in actin filament network via actin-binding activity, led to cytoplasmic localization of ALCAM [25]. They concluded that α-catenin played a significant role in the cell surface localization of ALCAM and its membranous localization by α-catenin, thereby enhanced a physiological function of ALCAM. In this regard, it should be noted that membranous ALCAM might be a more activated form that can interact with extracellular components because ALCAM, which consists of five extracellular domains, seems to fulfill its original function

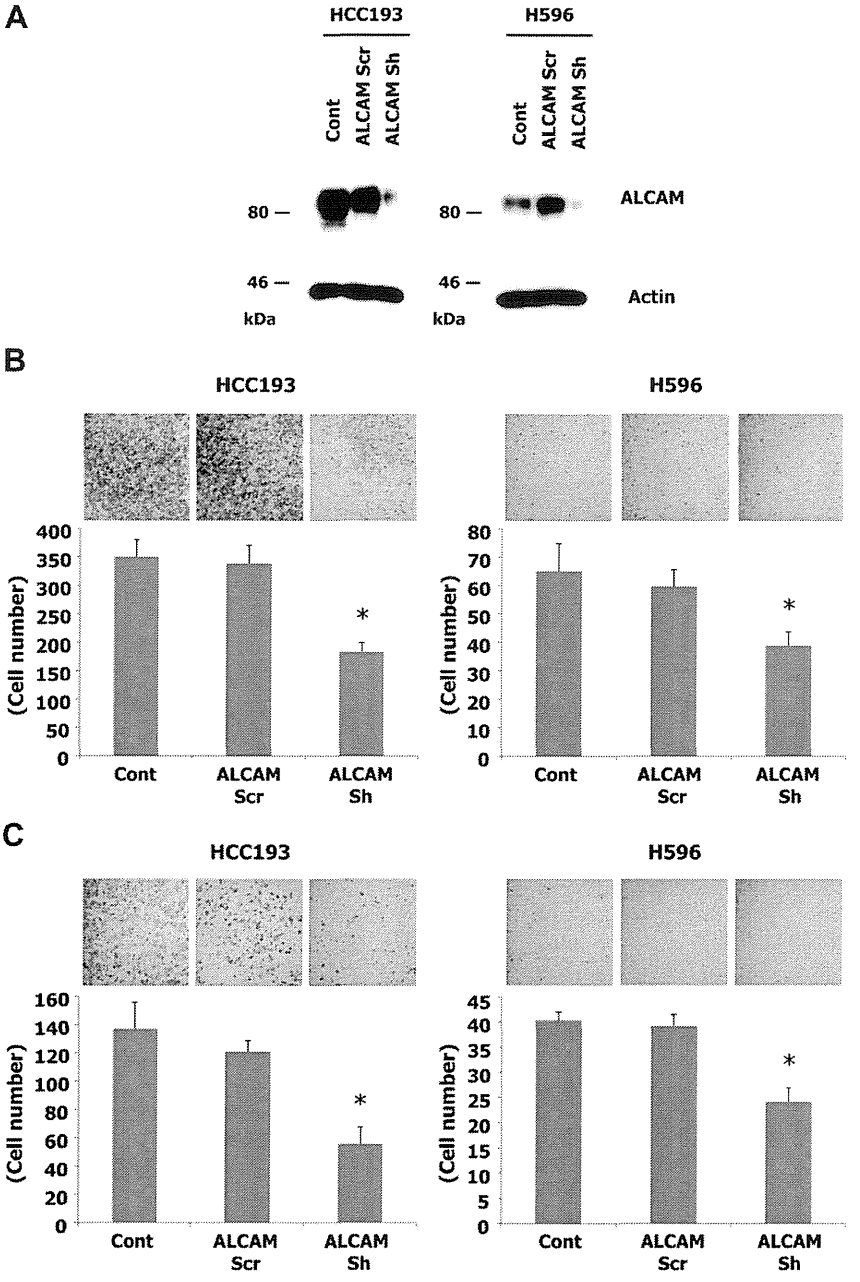

Fig. 4 – Lentiviral short hairpin RNA–mediated ALCAM knockdown in two NSCLC cell lines, HCC193 and H596. (A) Western blot analysis demonstrates the efficiency of ALCAM knockdown. The ALCAM-Sh vectors, ALCAM Sh, showed effective suppression of the level of ALCAM protein, whereas the control vectors, ALCAM Scr, showed no downregulation. Cells were lysed 96 h after infection. (B) ALCAM knockdown inhibited migration of two NSCLC cell lines. (C) ALCAM knockdown inhibited invasion of two NSCLC cell lines. The results of the triplicate experiments are presented. Columns, mean and bars, standard deviation. *$P < 0.05$ *versus* control.

as its homophilic interaction. However, it also remains to determine whether cytoplasmic ALCAM may have any other cancer-promoting function in cells including lung cancer.

ALCAM-mediated cell–cell adhesion was reported to promote matrix metalloprotease (MMP) activation in malignant melanoma cell lines [26]. They showed that ALCAM was involved in a regulatory role of MMP activity, which promotes proteolysis related to cancer invasion. Overexpression of MMPs was also described in resected NSCLC [27], and we found ALCAM promoted cell invasion *in vitro*. Taken together, these findings might imply that the positive role of ALCAM that leads to progression and metastases of NSCLC might be coupled to the increased activity of MMP.

In conclusion, our study suggested that membranous ALCAM expression was associated with the poor survival of patients with NSCLC. It also suggested that membranous ALCAM expression enhanced motility and invasion capacity of NSCLC cells *in vitro*. In this regard, patients whose tumor

has proved to be positive for membranous ALCAM expression, even if they have early-stage NSCLC, may well be considered for more careful management including adjuvant chemotherapy to improve their estimated poor outcome. Further studies are warranted to define the mechanism of ALCAM expression, which might also provide new insights into the better understanding of cell adhesion and progressive invasiveness of NSCLC cells.

Acknowledgment

The authors thank Mika Yamamoto and Tsutsumi Koike for their excellent technical assistance.

Sources of funding: This work is supported by a grant-in-aid for Scientific Research (B) from Japan Society for the Promotion of Science (22300338), a grant-in-aid for Third-Term Comprehensive Control Research for Cancer from the Ministry of Health, Labor and Welfare of Japan, and the Takeda Science Foundation.

Disclosures: None declared.

REFERENCES

[1] Jemal A, Bray F, Center MM, et al. Global cancer statistics. CA Cancer J Clin 2011;61:69.
[2] Sawabata N, Miyaoka E, Asamura H, et al. Japanese lung cancer registry study of 11,663 surgical cases in 2004: demographic and prognosis changes over decade. J Thorac Oncol 2011;6:1229.
[3] Oldenhuis CN, Oosting SF, Gietema JA, et al. Prognostic versus predictive value of biomarkers in oncology. Eur J Cancer 2008;44:946.
[4] van Kempen LC, Nelissen JM, Degen WG, et al. Molecular basis for the homophilic activated leukocyte cell adhesion molecule (ALCAM)-ALCAM interaction. J Biol Chem 2001;276:25783.
[5] van Kilsdonk JW, Wilting RH, Bergers M, et al. Attenuation of melanoma invasion by a secreted variant of activated leukocyte cell adhesion molecule. Cancer Res 2008;68:3671.
[6] Heffron DS, Golden JA. DM-GRASP is necessary for nonradial cell migration during chick diencephalic development. J Neurosci 2000;20:2287.
[7] Ikeda K, Quertermous T. Molecular isolation and characterization of a soluble isoform of activated leukocyte cell adhesion molecule that modulates endothelial cell function. J Biol Chem 2004;279:55315.
[8] Weidle UH, Eggle D, Klostermann S, Swart GW. ALCAM/CD166: cancer-related issues. Cancer Genomics Proteomics 2010;7:231.
[9] van Kempen LC, van den Oord JJ, van Muijen GN, et al. Activated leukocyte cell adhesion molecule/CD166, a marker of tumor progression in primary malignant melanoma of the skin. Am J Pathol 2000;156:769.
[10] Weichert W, Knösel T, Bellach J, et al. ALCAM/CD166 is overexpressed in colorectal carcinoma and correlates with shortened patient survival. J Clin Pathol 2004;57:1160.
[11] Ishigami S, Ueno S, Arigami T, et al. Clinical implication of CD166 expression in gastric cancer. J Surg Oncol 2011; 103:57.
[12] Kahlert C, Weber H, Mogler C, et al. Increased expression of ALCAM/CD166 in pancreatic cancer is an independent prognostic marker for poor survival and early tumour relapse. Br J Cancer 2009;101:457.
[13] King JA, Ofori-Acquah SF, Stevens T, et al. Activated leukocyte cell adhesion molecule in breast cancer: prognostic indicator. Breast Cancer Res 2004;6:478.
[14] Tomita K, van Bokhoven A, Jansen CF, et al. Activated leukocyte cell adhesion molecule (ALCAM) expression is associated with poor prognosis for bladder cancer patients. UroOncology 2003;3:121.
[15] Mezzanzanica D, Fabbi M, Bagnoli M, et al. Subcellular localization of activated leukocyte cell adhesion molecule is a molecular predictor of survival in ovarian carcinoma patients. Clin Cancer Res 2008;14:1726.
[16] Verma A, Shukla NK, Deo SV, et al. MEMD/ALCAM: a potential marker for tumor invasion and nodal metastasis in esophageal squamous cell carcinoma. Oncology 2005; 68:462.
[17] Sawhney M, Matta A, Macha MA, et al. Cytoplasmic accumulation of activated leukocyte cell adhesion molecule is a predictor of disease progression and reduced survival in oral cancer patients. Int J Cancer 2009;124:2098.
[18] Goldstraw P. Staging manual in thoracic oncology. Denver: IASLC; 2009.
[19] Travis WD, Brambilla E, Muller-Hermelink H, et al. Pathology and genetics of tumours of the lung, pleura, thymus and heart. Lyon: IARC Press; 2004.
[20] Kawaguchi K, Murakami H, Taniguchi T, et al. Combined inhibition of MET and EGFR suppresses proliferation of malignant mesothelioma cells. Carcinogenesis 2009;30:1097.
[21] Murakami H, Mizuno T, Taniguchi T, et al. LATS2 is a tumor suppressor gene of malignant mesothelioma. Cancer Res 2011;71:873.
[22] Soltermann A, Ossola R, Kilgus-Hawelski S, et al. N-glycoprotein profiling of lung adenocarcinoma pleural effusions by shotgun proteomics. Cancer 2008;114:124.
[23] Zhang WC, Shyh-Chang N, Yang H, et al. Glycine decarboxylase activity drives non-small cell lung cancer tumor-initiating cells and tumorigenesis. Cell 2012;148:259.
[24] Sudhir PR, Chen CH, Kumari MP, et al. Label-free quantitative proteomics and N-glycoproteomics analysis of KRAS-activated human bronchial epithelial cells. Mol Cell Proteomics; 2012 Jul 3 [Epub ahead of print].
[25] Tomita K, van Bokhoven A, Jansen CF, et al. Coordinate recruitment of E-cadherin and ALCAM to cell-cell contacts by alpha-catenin. Biochem Biophys Res Commun 2000;267:870.
[26] Lunter PC, van Kilsdonk JW, van Beek H, et al. Activated leukocyte cell adhesion molecule (ALCAM/CD166/MEMD), a novel actor in invasive growth, controls matrix metalloproteinase activity. Cancer Res 2005;65:8801.
[27] Cox G, Jones JL, O'Byrne KJ. Matrix metalloproteinase 9 and the epidermal growth factor signal pathway in operable non-small cell lung cancer. Clin Cancer Res 2000;6:2349.

Carcinogenesis vol.35 no.1 pp.164–172, 2014
doi:10.1093/carcin/bgt267
Advance Access publication July 19, 2013

Cancer-promoting role of adipocytes in asbestos-induced mesothelial carcinogenesis through dysregulated adipocytokine production

Shan Hwu Chew[1], Yasumasa Okazaki[1], Hirotaka Nagai[1,2], Nobuaki Misawa[1], Shinya Akatsuka[1], Kyoko Yamashita[1], Li Jiang[1], Yoriko Yamashita[1], Michio Noguchi[3], Kiminori Hosoda[3,4], Yoshitaka Sekido[5], Takashi Takahashi[6] and Shinya Toyokuni[1,*]

[1]Department of Pathology and Biological Responses, Nagoya University Graduate School of Medicine, Nagoya 466-8550, Japan, [2]Department of Pathology and Biology of Diseases, [3]Department of Endocrinology and Metabolism and [4]Faculty of Human Health Science, Kyoto University Graduate School of Medicine, Kyoto 606-8315, Japan, [5]Division of Molecular Oncology, Aichi Cancer Center Research Institute, Nagoya 464-8681, Japan and [6]Department of Molecular Carcinogenesis, Nagoya University Graduate School of Medicine, Nagoya 466-8550, Japan

*To whom correspondence should be addressed. Tel: +81 52 744 2086; Fax: +81 52 744 2091;
Email: toyokuni@med.nagoya-u.ac.jp

Like many other human cancers, the development of malignant mesothelioma is closely associated with a chronic inflammatory condition. Both macrophages and mesothelial cells play crucial roles in the inflammatory response caused by asbestos exposure. Here, we show that adipocytes can also contribute to asbestos-induced inflammation through dysregulated adipocytokine production. 3T3-L1 preadipocytes were differentiated into mature adipocytes prior to use. These cells took up asbestos fibers (chrysotile, crocidolite and amosite) but were more resistant to asbestos-induced injury than macrophages and mesothelial cells. Expression microarray analysis followed by reverse transcription–PCR revealed that adipocytes respond directly to asbestos exposure with an increased production of proinflammatory adipocytokines [e.g. monocyte chemoattractant protein-1 (MCP-1)], whereas the production of anti-inflammatory adipocytokines (e.g. adiponectin) is suppressed. This was confirmed in epididymal fat pad of mice after intraperitoneal injection of asbestos fibers. Such dysregulated adipocytokine production favors the establishment of a proinflammatory environment. Furthermore, MCP-1 marginally promoted the growth of MeT-5A mesothelial cells and significantly enhanced the wound healing of Y-MESO-8A and Y-MESO-8D human mesothelioma cells. Our results suggest that increased levels of adipocytokines, such as MCP-1, can potentially contribute to the promotion of mesothelial carcinogenesis through the enhanced recruitment of inflammatory cells as well as a direct growth and migration stimulatory effect on mesothelial and mesothelioma cells. Taken together, our findings support a potential cancer-promoting role of adipocytes in asbestos-induced mesothelial carcinogenesis.

Introduction

Malignant mesothelioma, which arises from the mesothelial cells lining the pleural, peritoneal and pericardial cavity, is closely associated with exposure to asbestos fibers. The first convincing evidence of an etiologic relationship between asbestos fibers and malignant mesothelioma emerged in 1960 (1). Since then, there has been considerable interest in unraveling the mechanisms underlying asbestos-induced mesothelial carcinogenesis. Macrophages were the first to receive great attention, as asbestos exposure is often associated with a chronic granulomatous inflammatory response. Several groups reported the activation of macrophages by asbestos fibers, and they showed that asbestos fibers were able to induce macrophages to release a multitude of factors, such as lysosomal enzymes, cytokines, plasminogen activators and reactive oxygen species (2–4), which collectively contribute to chronic inflammation. Subsequent studies revealed a direct interaction between asbestos fibers and mesothelial cells, and asbestos fibers were shown to be able to activate certain signaling cascades within mesothelial cells. This activation might be critical for mesothelial transformation (5–8). In addition, mesothelial cells themselves also play a role in the inflammatory response. Mesothelial cells are particularly sensitive to the cytotoxic effect of asbestos fibers. Yang *et al.* (9) termed the process of asbestos-induced mesothelial cell death as 'programmed necrosis', and they reported that during this process, there was an extensive release of high-mobility group box 1 into the extracellular space, which then initiated a chronic inflammatory response by inducing the macrophages to release tumor necrosis factor-α. Together, this evidence strongly supports the vital role of chronic inflammation in asbestos carcinogenicity.

To establish an animal model of mesothelioma, asbestos fibers are usually injected into the pleural or peritoneal cavity (10–12). According to some previous reports, the peritoneal cavity appeared to be more sensitive to the effect of asbestos fibers compared with the pleural cavity, i.e. malignant mesothelioma developed more frequently and rapidly in the peritoneal cavity following asbestos injection (13,14). We speculated that this finding might be related to the abundance of adipose tissue in the peritoneal cavity. A substantial body of recent evidence has revealed the role of adipose tissue in inflammation, particularly in obesity-related inflammation (15–17). This inflammatory response in the adipose tissue of obese individuals is linked to the development of type 2 diabetes mellitus.

Adipose tissue is now recognized as an endocrine organ that is capable of secreting a wide variety of biologically active peptides collectively known as adipocytokines [e.g. monocyte chemoattractant protein-1 (MCP-1), interleukin-6 (IL-6), leptin, adiponectin, plasminogen activator inhibitor-1 (PAI-1), resistin and visfatin]. Evidence from numerous epidemiologic studies has revealed an increased risk of cancer development in obese individuals, further supporting a cancer-promoting role of adipose tissue (18–21). Obesity has been defined as a low-grade chronic inflammatory condition. Many groups have reported that the dysregulated endocrine function of adipose tissue underlies this obesity-related inflammation (22–25). Dysregulation of adipose tissue generally results in the enhanced production of proinflammatory adipocytokines and suppression of anti-inflammatory adipocytokines.

Some previous studies have demonstrated the ability of adipocytes to perform phagocytosis in a macrophage-like manner (26,27). A direct interaction between asbestos fibers and adipocytes involving fiber internalization is thus very likely to take place. We hypothesized that this interaction can trigger off an inflammatory response in adipocytes which occurs through dysregulation of adipocytokine production, as in obesity. Due to the close anatomic proximity between adipocytes and mesothelial cells, altered levels of adipocytokines can potentially affect mesothelial cells in a paracrine manner. We performed this study to evaluate the potential involvement of adipose tissue as a cancer promoter in asbestos-induced carcinogenesis through its ability to aggravate the inflammatory response.

Abbreviations: Ccl, chemokine C-C motif ligand; FBS, fetal bovine serum; IL-6, interleukin-6; MCP-1, monocyte chemoattractant protein-1; mRNA, messenger RNA; MTT, thiazolyl blue tetrazolium bromide; NT-tngl, tangled carbon nanotubes; PAI-1, plasminogen activator inhibitor-1; Prl2c5, prolactin family 2, subfamily c, member 5; RT–PCR, reverse transcription–PCR.

Materials and methods

Materials

Three types of Union for International Cancer Control asbestos fibers (chrysotile A, crocidolite and amosite) were suspended in physiological saline. Tangled carbon nanotubes (NT-tngl, diameter = 15 nm; VGCF-X, Showa Denko, Tokyo, Japan) were suspended in physiological saline containing 0.5% bovine serum albumin. The 3T3-L1 preadipocyte cell line was a kind gift from Dr M.N. and Prof. K.H. (Kyoto University, Kyoto, Japan). MeT-5A and RAW264.7 cell lines were obtained from American Type Culture Collection (Manassas, VA). Y-MESO-8A and Y-MESO-8D cell lines were kindly provided by Prof. Y.S. (Aichi Cancer Centre Research Institute, Nagoya, Japan). These two human mesothelioma cell lines were established from the same Japanese patient with biphasic-like characteristics of malignant pleural mesothelioma and they showed epithelial and sarcomatous phenotypes, respectively, in cell culture (28). Recombinant human MCP-1 was purchased from PeproTech (Rocky Hill, NJ). Thiazolyl blue tetrazolium bromide (MTT) was purchased from Sigma (St Louis, MO). Dimethyl sulfoxide was purchased from Wako (Osaka, Japan).

Cell culture

3T3-L1 preadipocytes were maintained in Dulbecco's modified Eagle's medium supplemented with 10% calf serum and antibiotics. The differentiation of these preadipocytes into mature adipocytes was induced with Dulbecco's modified Eagle's medium supplemented with 10% fetal bovine serum (FBS), 0.5 mM 3-isobutyl-1-methyl-xanthine, 0.25 μM dexamethasone and 1 μg/ml insulin. Mature adipocytes were used for experiments within 10–14 days after the induction of differentiation. The RAW264.7 macrophage cell line was maintained in Dulbecco's modified Eagle's medium supplemented with 10% FBS and antibiotics. MeT-5A, a human mesothelial cell line immortalized through transfection with the pRSV-T plasmid (an SV40 ori-construct containing the SV40 early region and the Rous sarcoma virus long terminal repeat), was maintained in M199 medium supplemented with 10% FBS, 10 ng/ml epidermal growth factor, 870 nM insulin, 400 nM hydrocortisone, 0.3% (vol/vol) trace element B and antibiotics. Y-MESO-8A and Y-MESO-8D cell lines were maintained in RPMI 1640 medium supplemented with 10% FBS and antibiotics. All the cells were cultured in a humidified incubator with 5% CO_2 at 37°C.

Experimental animals

For animal experiments, 8-week-old male ddY mice (Japan SLC, Hamamatsu, Shizuoka, Japan) were used. The animals were housed in a specific pathogen-free animal facility with 12 h light/12 h dark cycle and allowed free access to food (CE-2, CLEA Japan, Tokyo, Japan) and water. These mice were subjected to a single intraperitoneal injection of 2.5 mg of asbestos fibers and killed after 3 days via cervical dislocation. Physiological saline (0.9%) was injected as a control. After killing, the epididymal fat pad was harvested; half of it was fixed in 10% phosphate-buffered formalin for histological analysis, whereas the other half was snap-frozen in liquid nitrogen and kept at −80°C until further use. The animal experiment was approved by the Animal Experiment Committee of the Nagoya University Graduate School of Medicine.

Oil Red O staining of adipocytes

Adipocyte maturation from the preadipocyte cell line was confirmed by staining the lipid droplets that accumulated in the cytoplasm of adipocytes during maturation using the Oil Red O staining method. After washing the mature adipocytes with phosphate-buffered saline, the cells were fixed with 10% phosphate-buffered formalin for 2 h. After another washing step, Oil Red O solution was added, and the cells were incubated at 37°C for 5 min. Images were acquired using a Nikon Eclipse TS-100 microscope (Nikon, Tokyo, Japan).

Fiber uptake by adipocytes

The uptake of asbestos fibers by adipocytes was analyzed by both light microscopy and transmission electron microscopy. Cultured adipocytes were exposed to 10 μg/cm^2 of asbestos fibers, and 24 h later, the cells were harvested by trypsinization and centrifuged to generate a cell pellet. For light microscopy, cell block was prepared by fixing the cells with 10% phosphate-buffered formalin and subsequently processed into a paraffin-embedded cell block. Sections of 4 μm were stained with Kernechtrot staining and viewed under ×100 magnification using a BZ-9000 microscope (Keyence, Osaka, Japan) to detect fibers inside the cells. For electron microscopy, cells were fixed with phosphate buffer containing 2.5% glutaraldehyde and 2% paraformaldehyde, followed by fixation with 1% osmium tetroxide. The cells were then embedded in Epon resin and cut into 80 nm ultrathin sections with diamond knife. After staining with uranyl acetate and lead citrate, detection of fibers inside the cells was performed using JEM-1400EX transmission electron microscope (JEOL, Tokyo, Japan).

Cell viability assay

The cytotoxicity of asbestos fibers on adipocytes, MeT-5A and RAW264.7 macrophages was measured using a CellTiter-Glo Luminescent Cell Viability Assay (Promega, Madison, WI). Asbestos fibers were added to the cells at a concentration of 10 μg/cm^2. After 72 h of incubation, the number of viable cells was evaluated via the addition of the CellTiter-Glo Luminescent Cell Viability Assay reagent followed by chemiluminescence measurement using a PowerScan4 plate reader (DS Pharma Biomedical, Osaka, Japan).

Microarray-based gene expression analysis

Microarray analysis was performed using an Agilent SurePrint G3 Mouse GE 8x60K Microarray slide and Agilent's Low Input Quick Amp Labeling Kit (Agilent Technologies, Santa Clara, CA) according to Agilent's One-Color Microarray-Based Gene Expression Analysis protocol. In total, 200 ng of total RNA extracted from adipocytes exposed to asbestos fibers under the conditions stated above was used as the initial material. Amplified cRNA was labeled with Cy3-CTP. Hybridization was performed by placing the slide in a hybridization oven equipped with a rotator and set at 65°C for 17 h. After hybridization, the microarray slide was washed with GE Wash Buffer and scanned, and data were analyzed using GeneSpring GX 10.02.2 software (Agilent Technologies).

Quantitative real-time reverse transcription–PCR

Total RNA was isolated from the differentiated adipocyte cell line or adipose tissue using the RNeasy Lipid Tissue Mini Kit (Qiagen, Valencia, CA). Total RNA was then reversed transcribed into complementary DNA using the SuperScript III First-Strand Synthesis Kit (Invitrogen, Grand Island, NY). Gene expression levels were quantitatively measured using the Platinum SYBR Green qPCR SuperMix-UDG kit (Invitrogen) and analyzed with an Applied Biosystems Model 7300 Real Time PCR System (Applied Biosystems, Foster City, CA). The β-actin level was used to normalize the messenger RNA (mRNA) level of all genes examined. The primer sequences used were as follows: mouse IL-6, forward, 5′-CTTCTTGGGACTGATGCTGG-3′, reverse, 5′-CAGAATTGCCATTGCACAAC-3′ (product size 185 bp); mouse β-actin, forward, 5′-ACATCCCCCAAAGTTCTACAAA-3′, reverse, 5′-TGAGGGACTTCCTGTAACCACT-3′ (product size 132 bp); mouse adiponectin, forward, 5′-GCAGGCATCCCAGGACATCC-3′, reverse, 5′-TCCTTTCCTGCCAGGGGTTC-3′ (product size 186 bp); mouse MCP-1, forward, 5′-CAGTTAACGCCCCACTCACC-3′, reverse, 5′-TCCTTCTTGG GGTCAGCACA-3′ (product size 163 bp); mouse prolactin family 2, subfamily c, member 5 (Prl2c5), forward, 5′-AACAAGGAACAAGCCAGGCACA-3′, reverse, 5′-ACCCCGTTCTGGACTGCGTT-3′ (product size 188 bp); mouse leptin, forward, 5′-CCAGCAGCTGCAAGGTGCAAGA-3′, reverse, 5′-CCCTCTGCTTGGCGGATACCGA-3′ (product size 214 bp) and mouse PAI-1, forward, 5′-ATGTGCACCTCTCCGCCCTCA-3′, reverse, 5′-GCTGCTCTTGGTCGGAAAGACTTG-3′ (product size 213 bp).

MCP-1 enzyme-linked immunosorbent assay

Differentiated adipocytes in a 6-well plate were exposed to different types of asbestos fibers and NT-tngl at 10 μg/cm^2 for 72 h. The cell culture medium was then collected, and the concentration of MCP-1 secreted by adipocytes into the culture medium was measured using the Quantikine Mouse JE/MCP-1 Immunoassay Kit (R&D Systems, Minneapolis, MN). The immunoassay was performed according to the manufacturer's instructions.

Immunohistochemistry

Paraffin-embedded tissue sections were deparaffinized and rehydrated. Antigen retrieval was performed by heating the sections with microwave using 10 mM citrate buffer, pH 6.0. Endogenous peroxidase was inhibited by incubating the sections with 0.3% hydrogen peroxide in methanol for 30 min. Tissue sections were then blocked with normal goat serum and incubated with rabbit polyclonal primary antibody against mouse MCP-1 (ab7202, abcam, Tokyo, Japan) or IL-6 (ab6672; abcam). After washing with phosphate-buffered saline, sections were incubated with biotinylated goat anti-rabbit immunoglobulin G secondary antibody. Detection of antigen–antibody complexes was performed by incubating the sections with horseradish peroxidase-conjugated streptavidin followed by 3,3′-diaminobenzidine. Images were acquired using BZ 9000 microscope.

Measurement of adipocyte size

Images of epididymal adipose tissue sections were acquired using BZ 9000 microscope at ×40 magnification. Ten random fields were taken for each section from five animals per group. Cell surface area was measured using ImageJ software (NIH, Bethesda, MD).

Transwell migration assay

Cell culture inserts and 24-well companion tissue culture plates from BD Falcon (Franklin Lakes, NJ) were used for transwell migration assay. The

cell culture insert contains a porous membrane with an 8 μm pore size. RAW264.7 macrophages were seeded into the insert at a density of 2 × 10^5 cells/insert. Conditioned medium collected from adipocytes that were treated or untreated with asbestos fibers was added to the lower chamber of the 24-well tissue culture plate. The plate was incubated for 24 h, followed by staining of the migrated cells with May–Grunwald's and Giemsa stains. Images were acquired in 10 random fields, and the number of migrated cells was counted.

MTT cell proliferation assay

MeT-5A cells were seeded into a 96-well tissue culture plate at a density of 5 × 10^3 cells/well. These cells were serum starved for 24 h before being treated with recombinant human MCP-1 at a concentration of 100 and 500 ng/ml. After 72 h of treatment, cell proliferation was measured using MTT. The MTT compound was dissolved in phosphate-buffered saline at a concentration of 5 mg/ml, and 20 μl was then added to each well. Cells were incubated with MTT for 4 h to allow the reduction of MTT into purple formazan. Culture

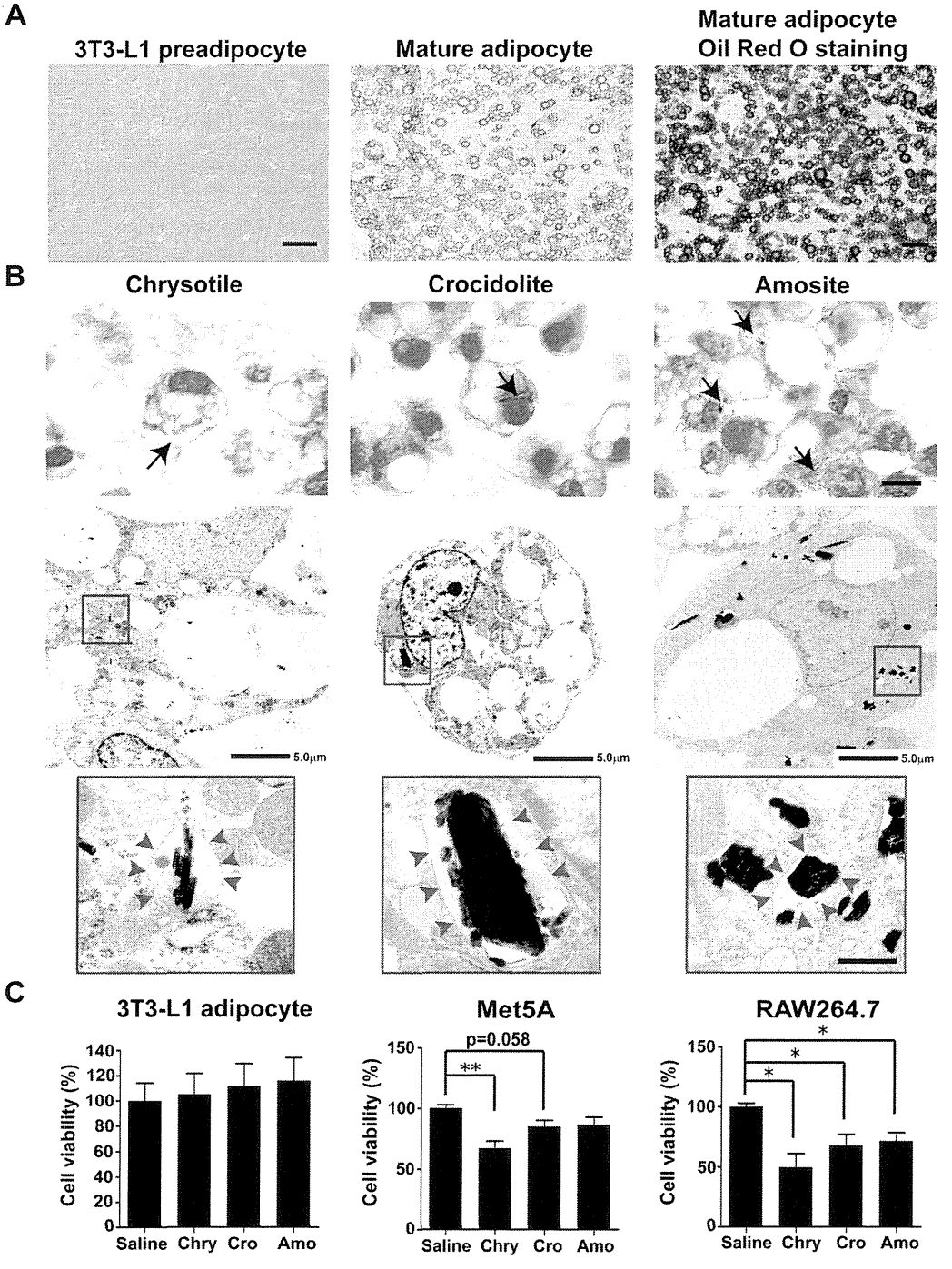

Fig. 1. Cultured adipocytes take up asbestos fibers but are resistant to their cytotoxic effect. (**A**) The 3T3-L1 preadipocyte cell line (left panel) was differentiated into mature adipocytes (middle panel) according to the standard differentiation protocol. Lipid droplets that accumulated in the mature adipocytes were stained by Oil Red O staining (right panel). Scale bars: left panel, 100 μm; middle and right panels, 20 μm. (**B**) The presence of asbestos fibers inside adipocytes was detected using light microscopy at ×100 magnification (upper panel) and transmission electron microscopy (middle and lower panels). Scale bars: upper panel, 10 μm; middle panel, 5 μm; lower panel, 500 nm. (**C**) The cytotoxicity of asbestos fibers on adipocytes, MeT-5A mesothelial cells and RAW264.7 macrophages was measured by the adenosine triphosphate cell viability assay. All the cells were exposed to 10 μg/cm^2 of asbestos fibers for 72 h. The results are shown as the mean ± SEM of three independent experiments. *$P \leq 0.05$, **$P \leq 0.005$. Amo, amosite; Chry, chrysotile; Cro, crocidolite.

medium containing MTT was then aspirated from the wells, followed by the addition of 100 µl of dimethyl sulfoxide into each well to dissolve the purple formazan crystals. The optical density was measured using a PowerScan4 plate reader.

Wound-healing assay

MeT-5A, Y-MESO-8A or Y-MESO-8D cells were grown in a 6-well tissue culture plate until the cells formed a confluent monolayer. A scratch was then made across the cell monolayer using a pipette tip. Recombinant human MCP-1 was added to some of the wells at a concentration of 500 ng/ml. Images of the wound were taken immediately after the scratch (designated as 0 h) and at 18, 24 and 48 h after the scratch. The width of the wound was measured using ImageJ software, and the percentage of wound healing was then calculated.

Statistical analysis

The statistical significance between two groups of interest was analyzed using the unpaired Student's *t*-test. A P value of <0.05 was considered significant.

Table I. Top 20 genes upregulated in asbestos-treated cultured adipocytes

Gene name	Accession number	Fold change
Top 20 genes upregulated in chrysotile-treated adipocytes		
Prolactin family 2, subfamily c, member 5 (Prl2c5)	NM_181852	18.596165
Fibrinogen-like protein-1 (Fgl1)	BC029734	8.48526
Chemokine (C-C motif) ligand 2 (Ccl2)	NM_011333	8.051252
Troponin T2, cardiac (Tnnt2), transcript variant 9	NM_011619	6.9297132
Prolactin family 2, subfamily c, member 1 (Prl2c1)	NM_001045532	6.292936
Secreted phosphoprotein 1 (Spp1)	NM_009263	5.334665
High-mobility group AT-hook 2 (Hmga2)	NM_010441	5.1633744
Chemokine (C-C motif) ligand 8 (Ccl8)	NM_021443	4.867768
lincRNA:chr19:9060613-9060851 forward strand		4.497705
Fos-like antigen 1 (Fosl1)	NM_010235	4.422233
Interleukin 1 receptor-like 1 (Il1rl1), transcript variant 1	NM_001025602	4.192457
Tumor necrosis factor receptor superfamily, member 9 (Tnfrsf9), transcript variant 1	NM_011612	4.0868807
Plasminogen activator, urokinase (Plau)	NM_008873	4.038391
Runt-related transcription factor 1 (Runx1), transcript variant 2	NM_001111022	3.8444314
Interleukin 1 receptor-like 1 (Il1rl1), transcript variant 2	NM_010743	3.7691207
cDNA sequence BC023744 (BC023744)	NM_001033311	3.6094844
Matrix metallopeptidase 10 (Mmp10)	NM_019471	3.6034727
Matrix metallopeptidase 13 (Mmp13)	NM_008607	3.5614529
Serine/threonine/tyrosine kinase 1 (Styk1)	NM_172891	3.4867864
Acyl-CoA synthetase bubblegum family member 1 (Acsbg1)	NM_053178	3.3379452
Top 20 genes upregulated in crocidolite-treated adipocytes		
Serum amyloid A 3 (Saa3)	NM_011315	21.692352
Haptoglobin (Hp)	NM_017370	11.54753
Dermokine (Dmkn), transcript variant 3	NM_001166173	9.095255
Suprabasin (Sbsn), transcript variant 1	NM_172205	7.677543
Secretory leukocyte peptidase inhibitor (Slpi)	NM_011414	6.6974707
Serine (or cysteine) peptidase inhibitor, clade A, member 3G (Serpina3g)	NM_009251	6.258521
PREDICTED: *Mus musculus* predicted gene, EG628900 (EG628900)	XM_893705	6.231637
Chemokine (C-C motif) ligand 2 (Ccl2)	NM_011333	5.961754
Chemokine (C-C motif) ligand 9 (Ccl9)	NM_011338	5.94364
Chitinase 3-like 1 (Chi3l1)	NM_007695	5.8167386
Lipocalin-2 (Lcn2)	NM_008491	5.732993
Chemokine (C-X-C motif) receptor 7 (Cxcr7)	NM_007722	5.6649795
Prolactin family 2, subfamily c, member 5 (Prl2c5)	NM_181852	5.511816
Complement component 4B (Childo blood group) (C4b)	NM_009780	5.504423
Serine (or cysteine) peptidase inhibitor, clade A, member 3H (Serpina3h)	NM_001034870	5.3198853
Runt-related transcription factor 1 (Runx1), transcript variant 4	NM_009821	5.090166
Triggering receptor expressed on myeloid cells 2 (Trem2)	NM_031254	4.8963866
Fibrinogen-like protein 1 (Fgl1)	NM_145594	4.8214192
Cannabinoid receptor 1 (brain) (Cnr1)	NM_007726	4.818088
Placental protein 11 related (Pp11r), transcript variant 2	NM_001168693	4.759451
Top 12 genes upregulated in amosite-treated adipocytes		
Extended synaptotagmin-like protein 3 (Esyt3)	NM_177775	2.988655
Budding uninhibited by benzimidazoles 1 homolog (*Saccharomyces cerevisiae*) (Bub1)	NM_009772	2.4976056
Potassium inwardly rectifying channel, subfamily J, member 6 (Kcnj6)	NM_001025585	2.4706264
lincRNA:chr4:21683562-21694344 reverse strand		2.4663801
PREDICTED: *M.musculus* predicted gene, EG666955 (EG666955)	XM_001000153	2.3627758
lincRNA:chr2:75493715-75494227 reverse strand		2.3625197
Adult male tongue cDNA, RIKEN full-length enriched library, clone:2310006M14 product:hypothetical protein, full insert sequence	AK009188	2.271196
ATPase, Ca^{++} transporting, type 2C, member 2 (Atp2c2)	NM_026922	2.2707396
lincRNA:chr6:31017987-31174287 reverse strand		2.2265513
Adult male olfactory brain cDNA, RIKEN full-length enriched library, clone:6430601O08 product:similar to Pol protein (fragment) (*M.musculus*), full insert sequence	AK032580	2.2096734
lincRNA:chr19:59498190-59531390 reverse strand		2.1915858
lincRNA:chr17:27479404-27481770 forward strand		2.082444

ATPase, adenosine triphosphatase; cDNA, complementary DNA. Twelve genes with >2-fold change were selected for amosite.

Results

Uptake of asbestos fibers by cultured adipocytes

The 3T3-L1 preadipocyte cell line was used to generate mature adipocytes according to the standard differentiation protocol. Adipocytes were used for subsequent experiments 10–14 days after the initiation of differentiation. During differentiation, the adipocytes accumulated lipid droplets in the cytoplasm that stained red upon Oil Red O staining (Figure 1A). Three different types of asbestos fibers, chrysotile, crocidolite and amosite fibers, were added to the adipocytes, followed by the assessment of fiber uptake using a cell block and light microscopy. Fiber uptake by the adipocytes was observed for all the asbestos types (Figure 1B, upper panel). Our findings were further supported by transmission electron microscopy, which clearly demonstrated fiber internalization by adipocytes (Figure 1B, lower panel). High magnification revealed the structure of a vesicular membrane around the asbestos fibers.

Asbestos fibers induce cell death when administered to mesothelial cells and macrophages (7,29). We compared the cytotoxicity of asbestos fibers on the cultured adipocytes, MeT-5A mesothelial cells and RAW264.7 macrophages by exposing them to the same concentration of asbestos fibers (10 μg/cm^2). When we performed an adenosine triphosphate detection cell viability assay on these different cell types, we did not observe any cytotoxic effect of asbestos fibers on the adipocytes, which was in contrast to mesothelial cells and macrophages (Figure 1C).

Cultured adipocytes showed changes in gene expression after asbestos exposure

As noted above, we hypothesized that the endocrine function of adipose tissue is potentially affected by asbestos exposure. To screen for genes with altered expression in asbestos-exposed adipocytes, we performed microarray gene expression analysis on the total RNA isolated from adipocytes after 72 h of exposure to asbestos fibers (GEO accession no.: GSE42330). The microarray results are shown in Table I. The top 20 genes that were upregulated in adipocytes after exposure to the different types of asbestos fibers are listed. More information can be found in the Supplementary Tables 1–3, available at *Carcinogenesis* Online. Gene expression analysis revealed the upregulation of some inflammation-related genes in adipocytes following exposure to asbestos fibers, including serum amyloid A3, haptoglobin and urokinase-type plasminogen activator. More importantly, we found the upregulation of an important adipocytokine that is commonly reported to be upregulated in obesity and is responsible for the related chronic inflammation and associated metabolic complications: chemokine C-C motif ligand 2 (Ccl2), which is also known as MCP-1. Other members of the C-C motif chemokine family were also upregulated, such as Ccl6, Ccl8 and Ccl9. Another gene that was upregulated in both chrysotile- and crocidolite-treated adipocytes was Prl2c5, which belongs to the prolactin superfamily.

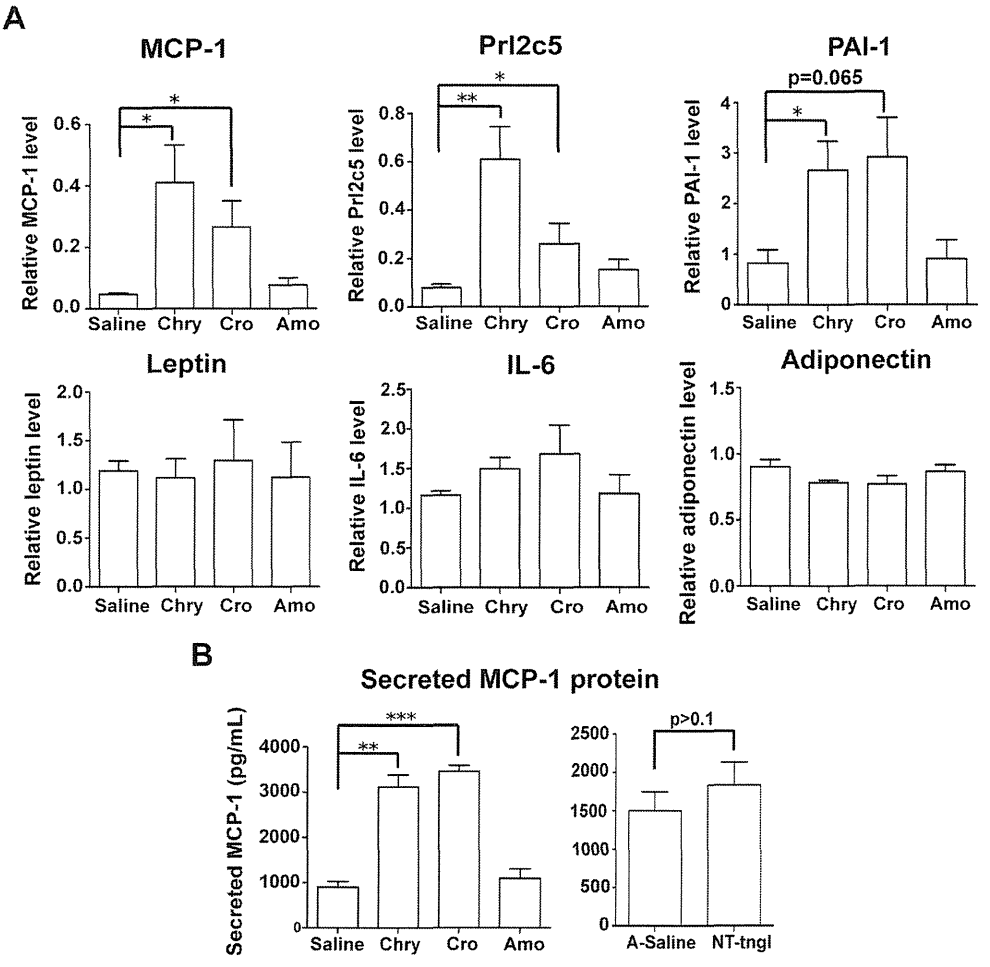

Fig. 2. Alterations in the expression level of adipocytokines in cultured adipocytes after asbestos exposure. Cultured adipocytes were exposed to chrysotile, crocidolite or amosite fibers at 10 μg/cm^2 for 72 h, with physiological saline as the control. (**A**) The gene expression level of various adipocytokines was measured by quantitative real-time RT–PCR and is shown relative to that of β-actin. (**B**) The secretion of MCP-1 into culture medium was measured by an MCP-1 immunoassay. In addition to asbestos fibers, adipocytes were also exposed to NT-tngl under the same experimental condition. The results are shown as the mean ± SEM of three independent experiments, $*P \leq 0.05$, $**P \leq 0.005$, $***P \leq 0.001$. Amo, amosite; A-Saline, saline containing 0.5% bovine serum albumin; Chry, chrysotile; Cro, crocidolite.

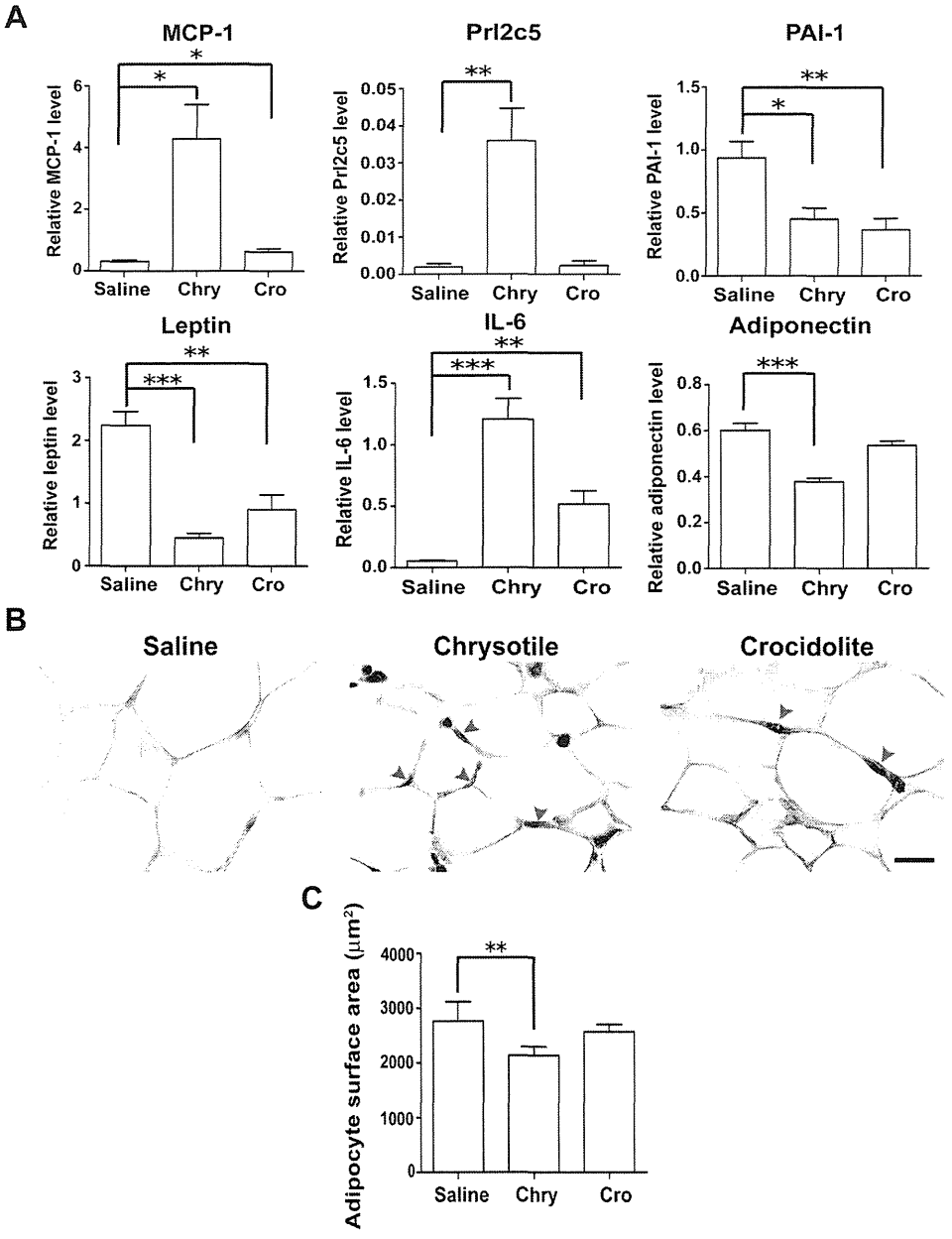

Fig. 3. Adipose tissues of mice injected with asbestos fibers show changes in adipocytokine expression levels. A total of 2.5 mg of chrysotile or crocidolite fibers was injected into the peritoneal cavity of mice, with physiological saline used as a control. Epididymal adipose tissue was harvested after 3 days. (**A**) The gene expression level of various adipocytokines in the epididymal adipose tissue was measured by quantitative real-time RT–PCR. The results are shown as the mean ± SEM ($n = 6$ per group). (**B**) Representative images of epididymal adipose tissue immunostained for MCP-1 expression. Scale bar: 20 μm. (**C**) Measurement of adipocyte cell surface area from adipose tissue sections using image analyzing software ($n = 5$ per group). $^{*}P \leq 0.05$, $^{**}P \leq 0.005$, $^{***}P \leq 0.001$. Chry, chrysotile; Cro, crocidolite.

MCP-1 was increased at the mRNA and protein level in adipocytes treated with asbestos fibers

Quantitative real-time reverse transcription–PCR (RT–PCR) was performed to evaluate the expression level of MCP-1, Prl2c5 and several other commonly known adipocytokines (PAI-1, leptin, IL-6 and adiponectin) in asbestos-treated or untreated adipocytes. In support of the microarray results, quantitative real-time RT–PCR showed the increased mRNA expression of MCP-1 and Prl2c5 in adipocytes following asbestos exposure (Figure 2A). Regarding the other adipocytokines examined, PAI-1 was also upregulated, whereas leptin, IL-6 and adiponectin did not show any significant alterations. Nevertheless, a slight decrease in adiponectin mRNA expression was observed. An enzyme-linked immunosorbent assay was performed to measure the secretion of MCP-1 protein into the culture medium of adipocytes treated with asbestos fibers. The enzyme-linked immunosorbent assay results corroborated those of quantitative real-time RT–PCR, showing a significant elevation of MCP-1 secretion by adipocytes treated with chrysotile and crocidolite fibers (control = 900.7 pg/ml, chrysotile treated = 3116.5 pg/ml, crocidolite treated = 3455.9 pg/ml, $P \leq 0.005$) (Figure 2B, left panel). Amosite-treated adipocytes did not show any apparent change in MCP-1 expression at either the mRNA or protein level. To determine whether any type of particulate is able to induce the same response, we also exposed the adipocytes to NT-tngl. Exposure to NT-tngl did not induce any significant increase in MCP-1 secretion from the adipocytes (Figure 2B, right panel).

Asbestos fibers dysregulated adipocytokine levels in adipose tissue of asbestos-exposed mice

To determine whether adipose tissue in living animals also responds to asbestos exposure, we injected chrysotile or crocidolite fibers into the peritoneal cavity of mice, with physiological saline as a control. Epididymal fat pads were harvested after 3 days, followed by quantitative real-time RT–PCR to examine changes in the expression level of adipocytokines. Again, the mRNA levels of MCP-1 and Prl2c5 were both upregulated in the adipose tissue of mice injected with asbestos fibers (Figure 3A). Regarding adiponectin, its suppressed expression level in the adipose tissue was more apparent than in the cultured adipocytes and was significant in chrysotile-injected mice. Leptin and IL-6 were significantly downregulated and upregulated, respectively, although no significant change in these two genes was observed in cultured adipocytes (Figure 2A). PAI-1 was the only exception that showed contradictory results between *in vitro* and *in vivo* assays. Immunohistochemical staining for MCP-1 and IL-6 was also performed on the adipose tissue sections. We found that in both chrysotile and crocidolite-injected mice, there was more intense MCP-1 staining in the cytoplasm of adipocytes compared with the saline-injected mice (Figure 3B). In contrast, the adipocytes did not show apparent positive staining of IL-6 (Supplementary Figure 1, available at *Carcinogenesis* Online), indicating that other inflammatory cells might be responsible for IL-6 mRNA upregulation as shown in Figure 3A. We have also noted some changes in adipocyte size and measurement of adipocyte surface area revealed a reduction of adipocyte size in asbestos-injected mice (Figure 3C).

MCP-1 promoted cancer cell phenotypes of mesothelial cells

Based on the well-known effect of MCP-1 as a macrophage chemoattractant, the increased secretion of MCP-1 by adipocytes in response to asbestos fibers might implicate an important indirect role of adipose tissue in enhancing the recruitment of macrophages to the sites of asbestos deposition. We collected culture media from asbestos-treated adipocytes and examined the ability of these conditioned media to induce macrophage migration. The transwell migration assay results revealed an increase in macrophage migration in response to the conditioned media from asbestos-treated adipocytes, which was most probably mediated by increased MCP-1 secretion (Figure 4).

Many chemokines have been reported to exert a mitogenic effect and are thus able to promote cancer development. We studied the effect of MCP-1 on mesothelial cell proliferation by treating MeT-5A cells with recombinant MCP-1 protein. MCP-1 showed a marginal but not significant effect on mesothelial cell proliferation (Figure 5A). In addition, we assayed the effect of MCP-1 on mesothelial cell migration. A wound-healing assay was performed in MeT-5A cells in the presence or absence of recombinant MCP-1 protein. We did not observe any effect of MCP-1 on MeT-5A cell migration (Figure 5B, left panel). However, we found that MCP-1 promoted the migration of the human mesothelioma cells Y-MESO-8A and Y-MESO-8D (Figure 5B, middle and right panels).

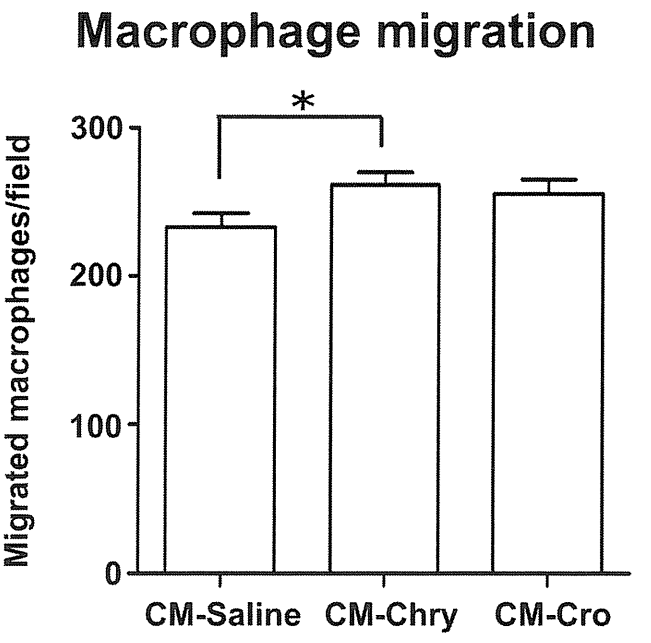

Fig. 4. Adipocytes induce increased macrophage migration following asbestos exposure. Cultured adipocytes were exposed to chrysotile or crocidolite fibers at 10 μg/cm^2 for 72 h, with physiological saline as a control. Conditioned medium was collected and assayed with a transwell migration assay to determine the ability of the conditioned media to induce macrophage migration. The results are shown as the mean ± SEM of three independent experiments. *$P \leq 0.05$. Chry, chrysotile; CM, conditioned medium; Cro, crocidolite.

Discussion

Our results revealed for the first time that asbestos fibers are able to directly affect the endocrine activity of adipocytes. This effect might be mediated through a direct interaction, as we showed that adipocytes were able to phagocytose asbestos fibers. Although adipose tissue is more abundant in the peritoneal cavity, it is also present in the pleural cavity, e.g. submesothelial space of the parietal pleura, around the pericardial sac and near the mediastinum (30,31). These anatomic locations render relevance of adipose tissue as it is accessible for the inhaled fibers through fiber translocation. In response to asbestos exposure, adipocytes upregulated proinflammatory adipocytokine such as MCP-1 but suppressed the level of anti-inflammatory adipocytokine, adiponectin, thereby shifting the balance towards a proinflammatory condition. Increased MCP-1 secretion by adipocytes might result in enhanced macrophage recruitment which in turn elaborates various cytokines and chemokines, leading to a vicious cycle that aggravates inflammation. Our results using adipocyte conditioned media to induce macrophage migration supported this notion. The role of adipose tissue in asbestos-induced inflammation can thus be both direct and indirect. MCP-1 has been reported to induce the proliferation of primary human pleural mesothelial cells (32) and our results using MeT-5A are consistent with the report. We also showed that MCP-1 promoted the migration of human mesothelioma cells. In addition, we observed a reduction in adipocyte size in asbestos-injected mice, which is probably due to the more active state of the adipocytes that requires higher metabolic rate.

MCP-1 transgenic and MCP-1$^{-/-}$ mice have previously been generated and characterized. MCP-1 overexpression in specific organs resulted in the enhanced recruitment of blood monocytes into the parenchyma of these organs (33,34). In contrast, in MCP$^{-/-}$ mice, there is a reduction in mononuclear cell infiltrate when these mice are challenged with different inflammatory stimuli (35). These mouse models are often used in studies related to obesity and insulin resistance. Kanda *et al.* (24) generated adipose-specific MCP-1 transgenic mice characterized by insulin resistance, hepatic steatosis and a higher degree of macrophage infiltration into adipose tissue. These MCP-1 genetically engineered mice might be a useful tool in our further studies to establish an association between MCP-1 expression and asbestos-induced mesotheliomagenesis.

In this study, we primarily focused on the possible tumor-promoting effects of MCP-1. Other adipocytokines with dysregulated expression might also play a cancer-promoting role. For instance, adiponectin expression is inversely correlated with human cancers. Low circulating levels of adiponectin have been associated with an increased risk of several cancers, such as colorectal cancer (36), endometrial cancer (37), postmenopausal breast cancer (38), gastric cancer (39) and prostate cancer (40). Adiponectin was reported to be able to inhibit the transcription factor nuclear factor-κB (41,42), which is

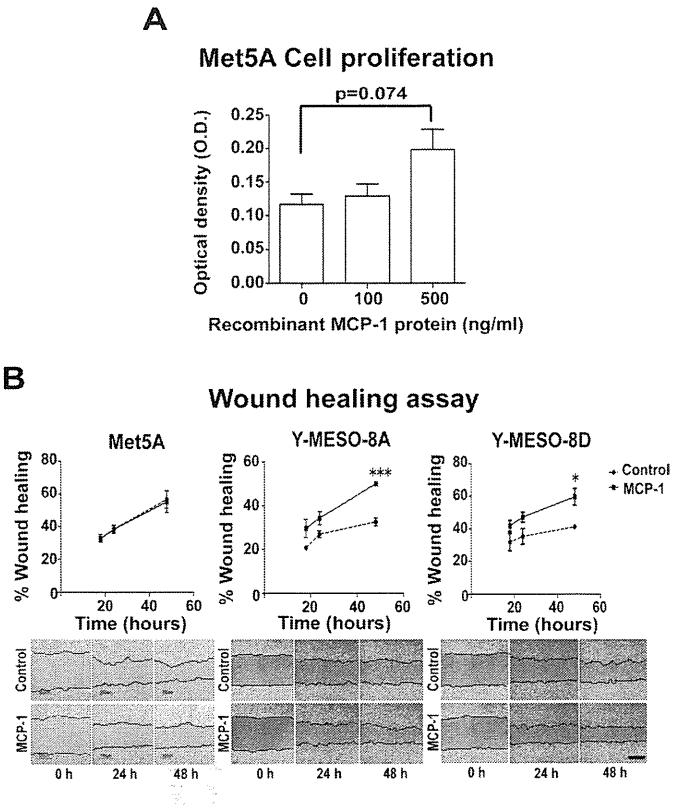

Fig. 5. Cancer-promoting effects of MCP-1. (**A**) Recombinant MCP-1 protein stimulates cell proliferation of the human mesothelial cell line MeT-5A, as measured by the MTT cell proliferation assay. (**B**) Recombinant MCP-1 protein induces the migration of the human mesothelioma cells Y-MESO-8A and Y-MESO-8D, as measured by the wound-healing assay. The results are shown as the mean ± SEM of three independent experiments. $^{*}P \leq 0.05$, $^{***}P \leq 0.001$.

a key molecule activated by asbestos fibers in mesothelial cells and macrophages that is responsible for inflammation. Our results suggested that asbestos fibers can cause a downregulation of adiponectin. The exact roles of leptin and PAI-1 in inflammation are still not entirely clear, although both were shown to be upregulated in obesity-related inflammation (43–45). A member of the prolactin superfamily, Prl2c5, was also upregulated. Current information regarding Prl2c5 is still relatively scarce, but this protein most probably shares many characteristics of prolactin, which is known to possess mitogenic property (46). Prolactin was newly found as an adipocytokine secreted by human adipose tissue (47,48). Several other genes more recently characterized as adipokines were also upregulated. Some of these genes, such as haptoglobin and lipocalin-2, bind to iron and can thus contribute to iron overload, which was shown to play an important role in asbestos-induced mesothelioma development (49). Another interesting upregulated peptide was secreted phosphoprotein 1, also known as osteopontin. Mesothelioma patients often have increased serum osteopontin levels and it was suggested to be a useful biomarker for the early diagnosis of mesothelioma (50). More detailed studies are needed to fully elucidate the potential pathogenic roles of these various dysregulated adipocytokines in mesothelial carcinogenesis. Moreover, a long-term study is needed to assess whether these alterations observed are long-term effects.

Interestingly, we found that chrysotile fibers appeared to be the most inflammogenic. Our results showed that chrysotile fibers dysregulated various adipocytokine levels to a higher extent than crocidolite and amosite fibers. This finding corroborates our recently published data that chrysotile fibers induced a significantly earlier development of malignant mesothelioma with intraperitoneal injection in rats compared with crocidolite and amosite fibers (49). The relatively stronger carcinogenicity of chrysotile fibers might be linked to a higher degree of adipose tissue inflammation. The reason underlying why chrysotile fibers seem to have a stronger inflammogenic effect on adipocytes is still not known, although our results showed that all types of asbestos fibers were internalized by the adipocytes.

To our knowledge, this is the first report of a potential association between dysregulated adipose endocrine function and asbestos-induced mesothelial carcinogenesis. We have shown that asbestos fibers are able to directly trigger an inflammatory response in adipocytes by dysregulating adipocytokine production. These adipocytokines might act locally to stimulate the growth/migration/survival of mesothelial cells and thus promote the development of malignant mesothelioma. The modulation of these adipocytokines might represent a novel strategy to extend the lifespan of mesothelioma patients.

Supplementary material

Supplementary Tables 1–3 and Figure 1 can be found at http://carcin.oxfordjournals.org/

Funding

Princess Takamatsu Cancer Research Fund (10-24213); Ministry of Health, Labour and Welfare of Japan (25-A-5); Ministry of Education, Culture, Sports, Science and Technology of Japan (24390094). The funders had no role in study design, data collection and analysis, decision to publish or preparation of the manuscript.

Conflict of Interest Statement: None declared.

References

1. Wagner,J.C. *et al.* (1960) Diffuse pleural mesothelioma and asbestos exposure in the North Western Cape Province. *Br. J. Ind. Med.*, **17**, 260–271.
2. Davies,P. *et al.* (1974) Asbestos induces selective release of lysosomal enzymes from mononuclear phagocytes. *Nature*, **251**, 423–425.
3. Hamilton,J.A. (1980) Macrophage stimulation and the inflammatory response to asbestos. *Environ. Health Perspect.*, **34**, 69–74.
4. Choe,N. *et al.* (1997) Pleural macrophage recruitment and activation in asbestos-induced pleural injury. *Environ. Health Perspect.*, **105** (suppl. 5), 1257–1260.
5. Ramos-Nino,M.E. *et al.* (2002) Mesothelial cell transformation requires increased AP-1 binding activity and ERK-dependent Fra-1 expression. *Cancer Res.*, **62**, 6065–6069.
6. Swain,W.A. *et al.* (2004) Activation of p38 MAP kinase by asbestos in rat mesothelial cells is mediated by oxidative stress. *Am. J. Physiol. Lung Cell. Mol. Physiol.*, **286**, L859–L865.
7. Yang,H. *et al.* (2006) TNF-alpha inhibits asbestos-induced cytotoxicity via a NF-kappaB-dependent pathway, a possible mechanism for asbestos-induced oncogenesis. *Proc. Natl Acad. Sci. USA*, **103**, 10397–10402.
8. Jagadeeswaran,R. *et al.* (2006) Functional analysis of c-Met/hepatocyte growth factor pathway in malignant pleural mesothelioma. *Cancer Res.*, **66**, 352–361.
9. Yang,H. *et al.* (2010) Programmed necrosis induced by asbestos in human mesothelial cells causes high-mobility group box 1 protein release and resultant inflammation. *Proc. Natl Acad. Sci. USA*, **107**, 12611–12616.
10. Whitaker,D. *et al.* (1984) Cytologic and tissue culture characteristics of asbestos-induced mesothelioma in rats. *Acta Cytol.*, **28**, 185–189.
11. Suzuki,Y. *et al.* (1984) Malignant mesothelioma induced by asbestos and zeolite in the mouse peritoneal cavity. *Environ. Res.*, **35**, 277–292.
12. Toyokuni,S. (2009) Mechanisms of asbestos-induced carcinogenesis. *Nagoya J. Med. Sci.*, **71**, 1–10.
13. Bolton,R.E. *et al.* (1982) Variations in the carcinogenicity of mineral fibres. *Ann. Occup. Hyg.*, **26**, 569–582.
14. Carthew,P. *et al.* (1992) Intrapleural administration of fibres induces mesothelioma in rats in the same relative order of hazard as occurs in man after exposure. *Hum. Exp. Toxicol.*, **11**, 530–534.
15. Fantuzzi,G. (2005) Adipose tissue, adipokines, and inflammation. *J. Allergy Clin. Immunol.*, **115**, 911–9; quiz 920.
16. Greenberg,A.S. *et al.* (2006) Obesity and the role of adipose tissue in inflammation and metabolism. *Am. J. Clin. Nutr.*, **83**, 461S–465S.
17. Itoh,M. *et al.* (2011) Adipose tissue remodeling as homeostatic inflammation. *Int. J. Inflam.*, **2011**, 720926.

18. Bianchini,F. *et al.* (2002) Overweight, obesity, and cancer risk. *Lancet Oncol.*, **3**, 565–574.
19. Calle,E.E. *et al.* (2003) Overweight, obesity, and mortality from cancer in a prospectively studied cohort of U.S. adults. *N. Engl. J. Med.*, **348**, 1625–1638.
20. Reeves,G.K. *et al.* Million Women Study Collaboration. (2007) Cancer incidence and mortality in relation to body mass index in the Million Women Study: cohort study. *BMJ*, **335**, 1134.
21. Renehan,A.G. *et al.* (2008) Body-mass index and incidence of cancer: a systematic review and meta-analysis of prospective observational studies. *Lancet*, **371**, 569–578.
22. Hotamisligil,G.S. *et al.* (1993) Adipose expression of tumor necrosis factor-alpha: direct role in obesity-linked insulin resistance. *Science*, **259**, 87–91.
23. Sartipy,P. *et al.* (2003) Monocyte chemoattractant protein 1 in obesity and insulin resistance. *Proc. Natl Acad. Sci. USA*, **100**, 7265–7270.
24. Kanda,H. *et al.* (2006) MCP-1 contributes to macrophage infiltration into adipose tissue, insulin resistance, and hepatic steatosis in obesity. *J. Clin. Invest.*, **116**, 1494–1505.
25. van Kruijsdijk,R.C. *et al.* (2009) Obesity and cancer: the role of dysfunctional adipose tissue. *Cancer Epidemiol. Biomarkers Prev.*, **18**, 2569–2578.
26. Cousin,B. *et al.* (1999) A role for preadipocytes as macrophage-like cells. *FASEB J.*, **13**, 305–312.
27. Villena,J.A. *et al.* (2001) Adipose tissues display differential phagocytic and microbicidal activities depending on their localization. *Int. J. Obes. Relat. Metab. Disord.*, **25**, 1275–1280.
28. Usami,N. *et al.* (2006) Establishment and characterization of four malignant pleural mesothelioma cell lines from Japanese patients. *Cancer Sci.*, **97**, 387–394.
29. Nagai,H. *et al.* (2011) Diameter and rigidity of multiwalled carbon nanotubes are critical factors in mesothelial injury and carcinogenesis. *Proc. Natl Acad. Sci. USA*, **108**, E1330–E1338.
30. Okby,N.T. *et al.* (2000) Liposarcoma of the pleural cavity: clinical and pathologic features of 4 cases with a review of the literature. *Arch. Pathol. Lab. Med.*, **124**, 699–703.
31. Shen,W. *et al.* (2003) Adipose tissue quantification by imaging methods: a proposed classification. *Obes. Res.*, **11**, 5–16.
32. Nasreen,N. *et al.* (2000) MCP-1 in pleural injury: CCR2 mediates haptotaxis of pleural mesothelial cells. *Am. J. Physiol. Lung Cell. Mol. Physiol.*, **278**, L591–L598.
33. Fuentes,M.E. *et al.* (1995) Controlled recruitment of monocytes and macrophages to specific organs through transgenic expression of monocyte chemoattractant protein-1. *J. Immunol.*, **155**, 5769–5776.
34. Gunn,M.D. *et al.* (1997) Monocyte chemoattractant protein-1 is sufficient for the chemotaxis of monocytes and lymphocytes in transgenic mice but requires an additional stimulus for inflammatory activation. *J. Immunol.*, **158**, 376–383.
35. Lu,B. *et al.* (1998) Abnormalities in monocyte recruitment and cytokine expression in monocyte chemoattractant protein 1-deficient mice. *J. Exp. Med.*, **187**, 601–608.
36. Wei,E.K. *et al.* (2005) Low plasma adiponectin levels and risk of colorectal cancer in men: a prospective study. *J. Natl Cancer Inst.*, **97**, 1688–1694.
37. Dal Maso,L. *et al.* (2004) Circulating adiponectin and endometrial cancer risk. *J. Clin. Endocrinol. Metab.*, **89**, 1160–1163.
38. Mantzoros,C. *et al.* (2004) Adiponectin and breast cancer risk. *J. Clin. Endocrinol. Metab.*, **89**, 1102–1107.
39. Ishikawa,M. *et al.* (2005) Plasma adiponectin and gastric cancer. *Clin. Cancer Res.*, **11** (2 Pt 1), 466–472.
40. Goktas,S. *et al.* (2005) Prostate cancer and adiponectin. *Urology*, **65**, 1168–1172.
41. Ajuwon,K.M. *et al.* (2005) Adiponectin inhibits LPS-induced NF-kappaB activation and IL-6 production and increases PPARgamma2 expression in adipocytes. *Am. J. Physiol. Regul. Integr. Comp. Physiol.*, **288**, R1220–R1225.
42. Wulster-Radcliffe,M.C. *et al.* (2004) Adiponectin differentially regulates cytokines in porcine macrophages. *Biochem. Biophys. Res. Commun.*, **316**, 924–929.
43. Auwerx,J. *et al.* (1988) Tissue-type plasminogen activator antigen and plasminogen activator inhibitor in diabetes mellitus. *Arteriosclerosis*, **8**, 68–72.
44. Juhan-Vague,I. *et al.* (1989) Increased plasminogen activator inhibitor activity in non insulin dependent diabetic patients–relationship with plasma insulin. *Thromb. Haemost.*, **61**, 370–373.
45. Hauner,H. (2005) Secretory factors from human adipose tissue and their functional role. *Proc. Nutr. Soc.*, **64**, 163–169.
46. Welsch,C.W. *et al.* (1977) Prolactin and murine mammary tumorigenesis: a review. *Cancer Res.*, **37**, 951–963.
47. Zinger,M. *et al.* (2003) Prolactin expression and secretion by human breast glandular and adipose tissue explants. *J. Clin. Endocrinol. Metab.*, **88**, 689–696.
48. Hugo,E.R. *et al.* (2008) Prolactin release by adipose explants, primary adipocytes, and LS14 adipocytes. *J. Clin. Endocrinol. Metab.*, **93**, 4006–4012.
49. Jiang,L. *et al.* (2012) Iron overload signature in chrysotile-induced malignant mesothelioma. *J. Pathol.*, **228**, 366–377.
50. Pass,H.I. *et al.* (2005) Asbestos exposure, pleural mesothelioma, and serum osteopontin levels. *N. Engl. J. Med.*, **353**, 1564–1573.

Received December 5, 2012; revised June 25, 2013; accepted July 31, 2013

Lung Cancer 83 (2014) 23–29

Contents lists available at ScienceDirect

Lung Cancer

journal homepage: www.elsevier.com/locate/lungcan

RASSF3 downregulation increases malignant phenotypes of non-small cell lung cancer

Asuki Fukatsu[a,d], Futoshi Ishiguro[a,e], Ichidai Tanaka[a,d], Takumi Kudo[g,h], Kentaro Nakagawa[g], Keiko Shinjo[a,b], Yutaka Kondo[a,c], Makiko Fujii[a], Yoshinori Hasegawa[d], Kenji Tomizawa[i], Tetsuya Mitsudomi[i,1], Hirotaka Osada[a,f], Yutaka Hata[g], Yoshitaka Sekido[a,f,*]

[a] Division of Molecular Oncology, Aichi Cancer Center Research Institute, 1-1 Kanokoden, Chikusa-ku, Nagoya 464-8681, Japan
[b] Division of Oncological Pathology, Aichi Cancer Center Research Institute, 1-1 Kanokoden, Chikusa-ku, Nagoya 464-8681, Japan
[c] Division of Epigenomics, Aichi Cancer Center Research Institute, 1-1 Kanokoden, Chikusa-ku, Nagoya 464-8681, Japan
[d] Department of Respiratory Medicine, Graduate School of Medicine, Nagoya University, Nagoya 466-8550, Japan
[e] Department of General Thoracic Surgery, Graduate School of Medicine, Nagoya University, Nagoya 466-8550, Japan
[f] Department of Cancer Genetics, Graduate School of Medicine, Nagoya University, Nagoya 466-8550, Japan
[g] Department of Medical Biochemistry, Graduate School of Medicine, Tokyo Medical and Dental University, Tokyo 113-8519, Japan
[h] Department of Neurosurgery, Graduate School of Medicine, Tokyo Medical and Dental University, Tokyo 113-8519, Japan
[i] Department of Thoracic Surgery, Aichi Cancer Center Hospital, 1-1 Kanokoden, Chikusa-ku, Nagoya 464-8681, Japan

ARTICLE INFO

Article history:
Received 12 February 2013
Received in revised form 5 September 2013
Accepted 21 October 2013

Keywords:
Non-small cell lung cancer
Lymph node metastasis
Pleural invasion
Tumor suppressor
RASSF3
EGFR

ABSTRACT

Background: Ras-Association Family1A (RASSF1A) is a well-established tumor suppressor. Ten RASSF homologues comprise this family, and each member is considered a tumor suppressor. RASSF3 is one of the RASSF family members, but its function has not yet been clarified. Recently, we found that RASSF3 interacts with MDM2 and facilitates its ubiquitination, which induces apoptosis through p53 stabilization. However, the role of RASSF3 in human malignancies remains largely unknown.
Patients and methods: Ninety-five non-small cell lung cancer (NSCLC) patients from Nagoya University Hospital and 45 NSCLC patients from Aichi Cancer Center Hospital underwent pulmonary resection at each hospital, and lung cancer and corresponding non-cancerous lung tissues were collected. The expression levels of *RASSF3* were analyzed using quantitative real-time reverse transcription PCR. We performed statistical analysis to investigate the correlation with *RASSF3* expression and the clinicopathological characteristics. We also transfected RASSF3-siRNA into NSCLC cells, and performed motility assays to evaluate the influence on migration ability.
Results: *RASSF3* expression levels were downregulated in 125 of a total 140 NSCLCs. In a multivariate logistic regression analysis, the low *RASSF3* expression group below the median value was independently correlated with progressive phenotypes (lymph node metastasis and pleural invasion), non-adenocarcinoma histology and wild-type epidermal growth factor receptor (EGFR) status. In motility assays, RASSF3-knockdown NSCLC cells increased the migration rate compared to the control cells.
Conclusions: We found that the expression levels of *RASSF3* were frequently downregulated in NSCLCs. Downregulation of *RASSF3* strongly correlated with the progressive phenotypes of NSCLCs and EGFR wild-type status. In vitro studies also suggested that *RASSF3* downregulation increases migration ability of lung cancer cells. Together, our findings indicate *RASSF3* is a candidate tumor suppressor gene of NSCLCs.

1. Introduction

Non-small cell lung cancer (NSCLC) is one of the most common human malignancies and its prognosis remains poor [1]. With the advance of molecular biology, various genetic/epigenetic alterations have been found to be associated with biological behaviors of human lung cancer cells.

Ten homologues, RASSF1 to RASSF10, comprise the RASSF family [2–5 review], which has drawn considerable attention over the

* Corresponding author at: Division of Molecular Oncology, Aichi Cancer Center Research Institute, 1-1 Kanokoden, Chikusa-ku, Nagoya 464-8681, Japan. Tel.: +81 52 764 2983; fax: +81 52 764 2993.
E-mail address: ysekido@aichi-cc.jp (Y. Sekido).
[1] Present address: Department of Thoracic Surgery, Kinki University Faculty of Medicine, 377-2 Ohno-Higashi, Osaka-Sayama 589-8511, Japan.

0169-5002/$ – see front matter © 2013 Elsevier Ireland Ltd. All rights reserved.
http://dx.doi.org/10.1016/j.lungcan.2013.10.014

last decade, because one member of this family, RASSF1A, is a well-established tumor suppressor [6,7]. *RASSF1A* has shown to be ubiquitously expressed in non-tumor lung tissues but frequently silenced in lung tumors due to CpG island methylation of its promoter [6–9]. The reexpression of *RASSF1A* in cancer cell lines led to suppress cell proliferation [6,7] and hypermethylation of the *RASSF1A* promoter region correlated with a poor prognosis and advanced stage of common malignancies [10–13].

RASSF1 to RASSF6 contains Ras-association (RA) domain in the C-terminus (C-terminal RASSF), whereas RASSF7 to RASSF10 have a RA domain in the N-terminus (N-terminal RASSF). Besides RASSF1A, other RASSF members have also been reported to be downregulated in several human cancers and considered as tumor suppressors. RASSF3, the smallest member of the C-terminal RASSF [14], was shown to be overexpressed in mammary gland of tumor-resistant mouse mammary tumor virus (MMTV)/neu mice compared to tumor-susceptible MMTV/neu littermates or non-transgenic mice [15]. Recently, we also found that exogenous RASSF3 directly interacts with MDM2 and facilitates its ubiquitination, which induces apoptosis through increasing p53 stability [16]. These data suggest that RASSF3 functions as a tumor suppressor like RASSF1A. However, the exact roles of RASSF3 in human malignancies and its clinicopathological features remain largely unknown. In this study, we found that the downregulation of RASSF3 expression was frequently observed in NSCLCs, which correlates with lymph node metastasis, pleural invasion, EGFR wild-type status and adenocarcinoma histology independently. We also found that the suppression of RASSF3 by siRNA in NSCLC cell lines increases cell motility.

2. Materials and methods

2.1. Clinical specimens

We studied two cohorts; 95 and 45 patients with NSCLC who underwent pulmonary resection at Nagoya University (NU) Hospital (March 2004–June 2006) and Aichi Cancer Center (ACC) Hospital (January 2006–December 2006), respectively. Characteristics of the patients at NU and ACC are listed in Supplementary Tables 1 and 2, respectively. The treatment policy was decided according to the standard protocol of each hospital, and fully informed written consent was obtained from all patients prior to tissue collection under ethical approval obtained at either hospital. Tumor samples from both hospitals and corresponding normal lung tissue samples (peripheral lung as distant from the cancerous lesions as possible) only from NU were snap frozen and stored at −80 °C.

2.2. RNA and DNA preparations and reverse transcription (RT)

Total RNA was extracted from tumor and non-tumor samples using an RNeasy Kit (Qiagen, Tokyo, Japan) according to the manufacturer's instructions. In NU cases, first strand cDNA was generated from a total RNA (1500 ng) extracted from grossly resected frozen tissues using SuperScript III (Invitrogen, Tokyo, Japan). In ACC cases, fresh tumor specimens were tapped on a slide glass, which left enriched tumor cells on the slide, and then total RNA was isolated, following first strand cDNA synthesis from a total RNA (2 ng) using High Capacity cDNA Reverse Transcription Kit (Applied Biosystems, Tokyo, Japan).

Genomic DNA was extracted using a QIAamp DNA Mini Kit (Qiagen) according to the manufacturer's instructions.

2.3. Statistical analysis

The clinicopathological characteristics of the patients were obtained from medical records. Overall survival (OS) and progression-free survival (PFS) was calculated from the date of pulmonary resection to the date of death and recurrence, respectively. Patients without the known date of death or recurrence were censored at the time of the last follow-up.

For comparisons of proportions, the χ^2 test was used. The Kaplan–Meier method was conducted to estimate the probability of survival as a function of time, and survival differences were analyzed using log-rank test. The logistic regression analysis was used to test for significant differences in *RASSF3* gene expression within multiple groups: such as age, sex, smoking history, TNM stage, size, lymph node metastasis, lymph and venous invasion, pleural invasion, and gene mutations. The level of significance was set at $p < 0.05$.

2.4. Wound healing assay

For wound healing assay, five cell lines (A549, HCC193, NCI-H23, VMRC-LCD, and BEAS-2B) were transfected with siRNA, re-plated to 3.5 cm dishes 48 h after transfection, and grown to confluence. The cells were damaged using 1–200 μl beveled orifice tip (Quality Scientific Plastics, San Diego, CA) and then allowed to migrate. Photographs were taken at the initial time, 12 and 24 h later. Three independent fields were recorded for each experiment. Migration rate was calculated as a – b/a (a and b represent the widths of the fissure at initial the time and each respective time point).

2.5. Transwell migration assay

The 3-dimension cell motility of five cell lines (A549, HCC193, NCI-H23, VMRC-LCD, and BEAS-2B) was measured with the transwell assay using a chamber containing the polyethylene terephthalate filter membrane with 8-μm pores (Falcon, Franklin Lakes, NJ). For each experiment, 48 h after siRNA transfection 1×10^5 transfected cells in 500 μl medium were seeded in the chamber, which was placed in 24-well plate containing 1 ml of RPMI1640 medium with 0.4% FCS. After incubation for 24 h, the chambers were fixed and stained using Diff Quick stain (Sysmex, Kobe, Japan). The numbers of migrated cells were counted using phase-contrast microscopy at ×200 magnifications in the three randomly selected fields.

2.6. Quantitative real-time RT-PCR

Quantitative real-time RT-PCR was performed on first strand cDNA using TaqMan probes and the TaqMan Gene Expression Master Mix (Applied Biosystems). TaqMan probes for *RASSF3* (Hs 00415584_m1) and *GAPDH* (Hs 03929097_g1) were purchased from Applied Biosystems and the amplification was performed on an ABI PRISM 7500 Fast real-time PCR system (Applied Biosystems). Quantification was performed in triplicate. The *RASSF3* expression was normalized with an internal control, *GAPDH* using Δ-ΔC_T method, and presented as a relative expression level using a ratio to the average of *RASSF3*/*GAPDH* of the mean of the 95 non-cancerous lung tissues, which was arbitrarily set at 1.

Additional materials and methods are described in the Supplementary Materials and Methods.

3. Results

3.1. RASSF3 expression significantly reduced in NSCLCs

To determine whether or not the *RASSF3* gene is involved in lung carcinogenesis, we first studied the *RASSF3* gene expression using 95 NSCLC samples with their corresponding normal lung tissue samples which we collected at Nagoya University (NU) Hospital (Fig. 1A and B). We found that most of the lung cancer tissues (87